

## **HIP1 is an Early-Stage Prognostic Biomarker of Lung Adenocarcinoma and Suppresses Metastasis via Akt-mediated EMT**

Che-Yu Hsu<sup>1#</sup>, Cheng-Han Lin<sup>2,3#</sup>, Yi-Hua Jan<sup>3</sup>, Chia-Yi Su<sup>3</sup>, Yun-Chin Yao<sup>4</sup>,  
Hui-Chuan Cheng<sup>2</sup>, Tai-I Hsu<sup>1</sup>, Po-Shun Wang<sup>2</sup>, Wen-Pin Su<sup>2</sup>, Chih-Jen Yang<sup>5</sup>,  
Ming-Shyan Huang<sup>5</sup>, Marcus J Calkins<sup>2</sup>, Michael Hsiao<sup>3\*</sup>, and Pei-Jung Lu<sup>1,2\*</sup>

<sup>1</sup>Institute of Basic Medical Sciences, College of Medicine, National Cheng Kung University, Tainan, Taiwan

<sup>2</sup>Institute of Clinical Medicine, College of Medicine, National Cheng Kung University, Tainan, Taiwan

<sup>3</sup>Genomics Research Center, Academia Sinica, Taipei, Taiwan

<sup>4</sup>Clinical Medicine Research Center, National Cheng Kung Hospital, Tainan, Taiwan

<sup>5</sup>Department of Internal Medicine, Kaohsiung Medical University Hospital, and School of Medicine, Kaohsiung Medical University, Kaohsiung, Taiwan

Supported by grants from National Research Program for Biopharmaceuticals of Taiwan (MOHW103-TDU-PB-211-133006) and National Health Research Institutes of Taiwan (NHRI-EX103-10152SI).

Author Contributions:

Designed study and interpreted data, C.-Y.H., C.-H.L., P.-J.L., and M.H.

Performed experiments, C.-Y.H., Y.-H.J., C.-H.L., Y.-C.Y., H.-C.C., T.-I.H., P.-S.W.,  
and C.-Y.S.

Provided materials, P.-J.L., M.H., W.-P.S., C.-J.Y., and M.-S.H.

Drafting the manuscript, C.-Y.H., C.-H.L., M.-J.C., and P.-J.L.

#C.-Y.H. and C.-H.L. contributed equally to this paper

\*Correspondence and requests for reprints should be addressed to:

Pei-Jung Lu, Ph.D., Institute of Clinical Medicine, College of Medicine, National  
Cheng Kung University, No.1, University Road, Tainan 70101, Taiwan. E-mail:  
pjlu2190@mail.ncku.edu.tw

Michael Hsiao, D.V.M., Ph.D., Genomics Research Center, Academia Sinica, 128  
Academia Road, Section 2, Nankang District, Taipei 115, Taiwan. E-mail:  
mhsiao@gate.sinica.edu.tw

**Running Title:** HIP1 suppresses metastasis of AdCA

### **At a Glance Commentary**

**Scientific Knowledge on the Subject:** Although the prognosis of non-small cell lung cancer (NSCLC) is very poor mainly due to regional or distant metastases, the molecular basis of metastases remains unclear.

**What This Study Adds to the Field:** In this study, we identify Huntingtin interacting protein-1 (HIP1) not only as an early-stage prognostic biomarker of AdCA, but also as a metastatic suppressor. Reduced expression HIP1 may lead to development of late metastases and cause a poor prognosis by modulating the Akt-mediated EMT signaling pathway. Our findings may lead to a novel application in prognostic evaluation of AdCA.

**Abstract**

**Rationale:** Non-small cell lung cancer (NSCLC) carries a poor survival rate mainly due to metastasis. However, the molecular mechanisms that govern NSCLC metastasis are undescribed. Huntingtin interacting protein-1 (HIP1) is known to play a role in tumorigenesis, we tested the involvement of HIP1 in NSCLC progression and metastasis.

**Objectives:** HIP1 expression was measured in human NSCLC tumors and correlation with survival outcome was evaluated. Furthermore, we investigated the ability of HIP1 to suppress a metastasis. The molecular mechanism by which HIP1 contributes to suppress metastasis was investigated.

**Methods:** We used tissue arrays containing samples from 121 NSCLC patients to analyze HIP1 expression by immunohistochemistry (IHC). In order to investigate the role of HIP1 expression on metastasis, we evaluated cellular mobility, migration and invasion using lung adenocarcinoma (AdCA) cells with modified HIP1 expression levels. The human disease mouse models with the same cells were applied to evaluate the HIP1 suppressing metastasis and its mechanism *in vivo*.

**Measurements and Main Results:** HIP1 expression in AdCA progression was found to be an early-stage prognostic biomarker, with low expression correlated to poor prognosis. We also found HIP1 to be a metastatic suppressor in AdCA. HIP1

significantly repressed the mobility of lung cancer cells both *in vitro* and *in vivo*, and regulated the epithelial-mesenchymal transition (EMT) by repressing AKT/GSK3 $\beta$ / $\beta$ -catenin signaling.

**Conclusions:** HIP1 serves as an early-stage prognostic biomarker and a metastatic suppressor. Reduced expression during AdCA progression can relieve HIP1 suppression of Akt-mediated EMT and thereby lead to development of late metastases and poor prognosis.

**Keywords:** HIP1; AdCA; prognosis; metastasis; EMT

## Introduction

Cancer is recognized globally as one of the most costly and deadly health problems, with lung cancer being the leading cause of cancer-related deaths (1, 2). Lung cancer is classified into two major categories according to histological criteria: non-small cell lung cancer (NSCLC, ~85%) and small cell lung cancer (SCLC, ~15%). NSCLCs are further categorized into three main subtypes by histopathology and clinical features: adenocarcinoma (AdCA, ~40%), squamous cell carcinoma (SCC, ~25-30%) and large cell carcinoma (LCC, ~10-15%). The prognosis for NSCLC patients is very poor, with a five-year survival rate of <1% (3-5). The poor survival rate is mainly attributable to regional or distant metastasis (6-9). Although metastasis is the principal event leading to lung cancer deaths, its molecular basis remains poorly understood.

Huntingtin interacting protein-1 (HIP1) is a 116-kDa protein (10, 11) that belongs to an evolutionarily conserved family, which also includes the yeast *Sla2p* (12, 13) and the mammalian HIP1-related (HIP1r) proteins (14, 15). HIP1 was reported to be a component of the clathrin-mediated endocytosis pathway because of its association with both the actin cytoskeleton and endocytosis machinery (16-20). Additionally, many studies have suggested that HIP1 plays a role in tumorigenesis by providing evidence of overexpression in various human malignancies and

transforming fibroblasts (21-28). Although HIP1 associates with human cancer biology, its precise role in tumor progression remains unknown (21).

The epithelial-mesenchymal transition (EMT) is a major developmental process, which has also been implicated in tumor progression (29). EMT allows benign tumor cells to infiltrate the surrounding tissue and ultimately metastasize to distant sites (30). EMT can be induced by growth factors such as transforming growth factor- $\beta$  (TGF- $\beta$ ) and epidermal growth factor (EGF). EMT is commonly detected by decreases in molecular markers of epithelium such as keratin intermediate filaments (cytokeratin), desmosomes (desmoplakin) and adherens junction proteins (E-cadherin and occludin), increases in mesenchymal markers such as Vimentin and N-cadherin, and increasing extracellular matrix (ECM) molecules such as fibronectin (31). Furthermore, nuclear localization of  $\beta$ -catenin and elevation of transcription factors such as Snail1 (Snail), Snail2 (Slug), Twist, EF1/ZEB1, SIP1/ZEB2 and/or E47 during EMT have also been reported (32). Phenotypic markers for EMT include an increased capacity for migration and three-dimensional invasion as well as resistance to anoikis/apoptosis (29). The mechanisms that govern EMT are now being unraveled, and studying these mechanisms may reveal promising targets for the prevention of metastasis (31).

Our study shows that HIP1 represents an early-stage AdCA prognostic biomarker and acts as a metastatic suppressor by inhibiting Akt-mediated EMT. The decreased

expression of HIP1 during AdCA progression allows upregulation of Akt activity to promote EMT, which is expected to facilitate tumor metastasis.

## **Methods**

A complete description of materials and methods is provided in the online supplement.

## **Results**

**HIP1 expression decreases during AdCA progression and represents an early-stage prognostic biomarker.**

To examine HIP1 expression during NSCLC progression, lung tissues were probed using immunohistochemistry (IHC). Specimens were divided into four groups based on NSCLC staging: normal, stage I, stage II/III, and stage IV. After IHC staining, the intensity of brown color, which reflects the level of HIP1 expression, was scored on a scale from 0 (no expression) to 3 (high expression) (Figures E1A and E1B). The percentage of low- (scores 0-1) and high-intensity (scores 2-3) samples was calculated in the four groups of specimens (Figures 1A and 1B). In the first cohort (n=121), the stage I group contained the highest percentage of high-intensity HIP1 samples, the stage II/III group contained the second most, the stage IV group

contained the third most, and the normal group contained the least. These results suggest that HIP1 expression is increased in early stage disease, but this increase is negatively correlated with NSCLC progression.

To investigate the correlation between HIP1 expression and NSCLC prognosis, Cox multivariate regression analysis was performed. This analysis showed that NSCLC patient survival was associated with the level of HIP1 expression and the N/M prognostic factors (Table 1). We also used a Kaplan-Meier log-rank analysis to show that the patients with low-level HIP1 expression demonstrated worse survival curves (Figures 1C and 1D). Moreover, we analyzed clinicopathologic characteristics of NSCLC patients with tumors showing low and high HIP1 expression (Table 2). HIP1 expression levels were correlated with overall survival rate and the occurrence of long-distance metastasis. Moreover, NSCLC patients showing low-level HIP1 mRNA expression in the Prognoscan database also exhibited poor survival (Figure E2 and Table E1). The correlation between the HIP1 expression level and the survival of NSCLC patients in early stages (stage I-II, n=52) (Figures 1E and 1F) was evaluated. HIP1 expression was associated with patient survival, and HIP1 represented a prognostic biomarker of the early-stage NSCLC. To clarify the correlation between HIP1 expression and NSCLC metastasis (Figure 1G), specimens were separated into two groups based on the clinical diagnosis of metastasis. The statistical comparison

showed that the percentage of low HIP1 expression in the group of metastasis was higher than non-metastasis. These results revealed that HIP1 expression was significantly correlated with NSCLC patient's survival and metastasis.

Because NSCLCs are mainly composed of AdCA and SCC, we analyzed HIP1 expression in normal and tumor tissues of these subtypes (Figure E1C). Increased HIP1 expression was found when comparing AdCA samples to normal alveolar epithelium, however, SCC samples did not exhibit increased HIP1 expression when compared to normal bronchial epithelium. We also found that the overall and disease-free survival were both associated with HIP1 expression in AdCA and SCC cases (Figures E1D-E1G). Additionally, in NSCLC patients receiving chemotherapy, low HIP1 expression presented worse survival curves (Figure E1H). Another two cohorts confirmed that HIP1 expression correlated with AdCA patient survival, but not SCC (Figures E1I-E1Q). Overall, these data indicate that decreased HIP1 expression is associated with poor prognosis in AdCA, but not SCC.

#### **HIP1 represses the mobility of AdCA cells *in vitro*.**

To study the correlation between HIP1 expression and AdCA cellular mobility, we evaluated endogenous HIP1 expression in various AdCA cell lines. According to Western blotting (WB) and IHC data (Figure E3A), we saw that HIP1 expression

exhibited a reverse association with AdCA cellular mobility. To clarify the roles of HIP1 in regulating AdCA cellular mobility, lung CL1 cell lines with well-characterized mobility were selected for evaluation. WB and RT-PCR (Figure 2A) showed that CL1-0 cells had the highest HIP1 levels when compared to CL1-2, CL1-3 and CL1-5 cells. Conversely, the migration and invasion assays (Figure 2B) revealed that CL1-0 cells possessed lower mobility than CL1-2, CL1-3 and CL1-5 cells. Collectively, HIP1 expression was inversely correlated with cellular mobility of the CL1 cells. To directly test whether HIP1 regulates cellular mobility, HIP1 was transiently manipulated in CL1-0 and CL1-5 cells (Figures E3B and E3C). Data obtained from WB, migration and invasion assays showed that knocking down HIP1 expression in CL1-0 cells promoted cellular mobility, whereas HIP1 overexpression in CL1-5 cells suppressed cellular mobility.

HIP1 knockdown was validated by WB in CL1-0, A549 and H441 cells, and similarly overexpression was validated in CL1-5, H928 and H1299 cells (Figures 2C, E4A, E5A, E6A, E7A). The MTT assay revealed that HIP1 knockdown in CL1-0 and A549 cells significantly inhibited cell growth, whereas HIP1 overexpression in CL1-5 and H1299 cells significantly promoted cell growth. In the wound-healing assay (Figures 2D, E4D, E5D, E6D, E7D), HIP1-knockdown in CL1-0, A549 and H441 cells led to greater migration, whereas HIP1-overexpressing CL1-5, H928 and H1299

cells exhibited less migration than controls. In migration and invasion assays (Figures 2E, E4EF, E5EF, E6EF, E7EF), HIP1-knockdown in CL1-0, A549 and H441 cells produced high cellular mobility, whereas HIP1-overexpression in CL1-5, H928 and H1299 cells led to reduced cellular mobility. To confirm that HIP1 regulated cellular mobility, transient HIP1 re-overexpression was performed in stable HIP1-knockdown CL1-0 cells, and conversely transient HIP1 re-knockdown was performed in stable HIP1-overexpressing CL1-5 cells. Data from migration and invasion assays (Figure 2F) showed that the CL1-0 shHIP1#1 and #2 cells that had rescued expression of HIP1 had relatively low mobility. In contrast, the CL1-5 HIP1 cells transfected with shHIP1#1 and #2 showed high mobility. Because endogenous HIP1 expression within H441 and H1299 cells was similar, we also performed transient HIP1 overexpression in H441 cells and transient HIP1 knockdown in H1299 cells to evaluate cellular mobility. The results of WB, migration and invasion assays (Figures E5GH and E7GH) showed that decreasing HIP1 expressions promoted cellular mobility, whereas increasing HIP1 expressions suppressed cellular mobility. Taken together, these results provide ample evidence that HIP1 suppresses cellular mobility in AdCA cells. Overall, we found that HIP1 promoted AdCA cell growth, but repressed cellular mobility *in vitro*.

**HIP1 acts as a metastatic suppressor of AdCA *in vivo*.**

To investigate whether HIP1 suppressed AdCA metastasis *in vivo*, animal experiments were performed by injecting mice either orthotopically or through the tail vein with stable HIP1-modified CL1 cells. Following orthotopic lung injection (Figure 3A), the CL1-0 shHIP1#1 group showed more metastatic tumor cells on the surface of right lungs compared to the CL1-0 scramble group. The CL1-5 Vec group showed more metastatic tumor cells on the surface of right lungs compared to the CL1-5 HIP1 group. According to hematoxylin and eosin (HE) staining, left lungs (receiving side) showed relatively large lung adenocarcinoma in all groups, and right lungs (CL1-0 shHIP1#1 or CL1-5 Vec group) had more metastatic tumor cells.

Following tail vein injection (Figure 3B), a similar result was observed. The CL1-0 shHIP1#1 group showed more metastatic tumor cells in mice lungs, whereas the CL1-5 HIP1 group showed fewer metastatic tumor cells. According to HE staining, mice receiving CL1-0 shHIP1#1 or CL1-5 Vec cells had more metastatic tumor cells in lung sections compared to mice receiving CL1-0 scramble or CL1-5 HIP1 cells. Notably, IHC against human mitochondria, a tracing marker to recognize injected human tumor cells in mice, in the CL1-5 groups using tail vein injection (Figure 3C) confirmed that more metastatic tumor cells appeared in the Vec group than the HIP1 group.

Distant metastasis to liver and kidneys was also observed in the orthotopic lung injection experiments (Figures E8A and E8B). More metastatic tumor cells appeared in livers from the groups of CL1-0 shHIP1#1 and CL1-5 Vec compared with CL1-0 scramble and CL1-5 HIP1. Kidneys from the CL1-5 Vec group also had more metastatic tumor cells than the CL1-5 HIP1 group. There were no significant differences in lung weight between the HIP1-knockdown CL1-0 and HIP1-overexpressing CL1-5 groups (Figure E8C). In summary, our orthotopic injection and tail vein injection data indicate that HIP1 suppressed AdCA metastasis *in vivo*.

#### **HIP1 inhibits AdCA Epithelial-Mesenchymal Transition.**

To explain how HIP1 regulated AdCA cellular mobility, cDNA microarray was used to identify the genes affected by stable HIP1-knockdown in CL1-0 cells (Figure 4A). The MetaCore statistical analysis showed that the significantly affected genes were mostly involved in EMT regulation (Figure 4B). These EMT-related genes were divided into two groups by color, with red indicating upregulated genes (mostly mesenchymal: M-markers) and green indicating downregulated genes (mostly epithelial: E-markers) under HIP1-knockdown conditions. CL1-0 cells are known as epithelial-like, and CL1-5 cells are mesenchymal-like. WB analysis (Figure 4C)

showed that CL1-2, CL1-3 and CL1-5 cells had less HIP1 and E-cadherin, but more  $\beta$ -catenin, Slug, Snail and Vimentin, compared with CL1-0 cells. After TGF $\beta$  (5 ng/ml) treatment (Figure 4D), WB data showed that E-cadherin and HIP1 decreased in A549 cells. These results suggest that HIP1 is involved in regulating EMT.

EMT-related gene expression was monitored in several HIP1-modified AdCA cells. In the HIP1-knockdown CL1-0, A549 and H441 cells (Figures 4E, E4BC, E5BC), qPCR data showed that E-cadherin and microphthalmia-associated transcription factor (MITF) expressions were downregulated, but Slug, Vimentin, plasminogen activator inhibitor-1 (PAI1), tumor necrosis factor receptor-1 (TNFR1) and matrix metalloproteinase-1 (MMP1) expressions were upregulated. The expression levels of Snail and focal adhesion kinase (FAK) were not affected. Moreover, WB data confirmed that HIP1 and E-cadherin expression were downregulated, but Slug and Vimentin expression were upregulated. The expression levels of  $\beta$ -catenin and Snail were not affected. In the HIP1-overexpressing CL1-5, H928 and H1299 cells (Figures 4F, E6BC, E7BC), qPCR and WB data showed the converse results compared with those from the HIP1-knockdown cells. The mRNA expression levels of Snail and FAK, and the protein expression levels of  $\beta$ -catenin and Snail were not affected. Collectively, these data suggest that HIP1 expression upregulated the expression levels of E-markers and downregulated the expressions of

M-markers.

Increased nuclear translocation of  $\beta$ -catenin is also a marker of EMT. Subcellular fractionation analysis was conducted (Figure 4G), and WB data showed that the cytoplasmic extracts of HIP1-knockdown CL1-0 cells contained less  $\beta$ -catenin, whereas the nuclear extracts contained more  $\beta$ -catenin compared with controls. In contrast, the cytoplasmic extracts of HIP1-overexpressing CL1-5 cells contained more  $\beta$ -catenin, whereas the nuclear extracts contained less  $\beta$ -catenin compared with controls. These results showed that HIP1 suppressed the nuclear translocation of  $\beta$ -catenin. Because the activity of transcription factor 4 (TCF4) is promoted by nuclear  $\beta$ -catenin, luciferase reporter assays were conducted to evaluate TCF4 activity (Figure 4H). The HIP1-knockdown CL1-0 cells showed high TCF4 activity, whereas the HIP1-overexpressing CL1-5 cells showed low TCF4 activity. These data indicated that HIP1 suppressed the activity of TCF4. In summary, HIP1 may suppress EMT by inhibiting the nuclear translocation of  $\beta$ -catenin, repressing TCF4 activity and decreasing the expression of Slug. This downregulation of Slug expression would be expected to correspond with low levels of mesenchymal markers but the high levels of epithelial markers, thereby preventing metastasis.

**HIP1 blocks the Akt-mediated EMT signaling pathway.**

In our studies, HIP1 regulated the nuclear translocation of  $\beta$ -catenin (Figure 4G) suggesting transcriptional regulation of Slug. Because the relative change in Slug at the protein level was more dramatic than that in the mRNA level (Figures 4E and 4F), we also evaluated whether HIP1 affected Slug post-translational modifications. Previous papers have reported that glycogen synthase kinase-3 $\beta$  (GSK3 $\beta$ ) regulates the nuclear translocation of  $\beta$ -catenin and the post-translational modification of Slug (33, 34). Therefore, we examined the Akt-GSK3 $\beta$  signaling pathway in HIP1 modified cell lines (Figure 5A). The HIP1-knockdown CL1-0 cells exhibited increased levels of pGSK3 $\beta$ -Ser9 and pAkt-Ser473, whereas the HIP1-overexpressing CL1-5 cells had decreased levels compared to control cells. The levels of phosphorylated pyruvate dehydrogenase kinase isozyme-1 (pPDK1-Ser241) were not affected. Similar results were found in HIP1-knockdown A549/H441 cells and the HIP1-overexpressing H928/H1299 cells (Figures E4C, E5C, E6C, E7C). These data revealed that HIP1 inhibited Akt activity and the Akt-GSK3 $\beta$  signal transduction. To confirm that HIP1 regulated EMT and the Akt-GSK3 $\beta$  signaling pathway, transient HIP1 rescue and depletion studies were performed. WB data (Figure 5B) showed that the CL1-0 shHIP1#1 and #2 cells that re-overexpressed HIP1 contained more HIP1 and E-cadherin, but less pAkt-Ser473, pGSK3 $\beta$ -Ser9, Slug and Vimentin. Expectedly, the CL1-5 HIP1 cells transfected with shHIP1#1 and #2 produced the converse results.

These data suggest that HIP1 suppression of cellular mobility may be due to inhibition of EMT through the Akt-GSK3 $\beta$  signaling pathway.

To confirm that HIP1 repressed the EMT and cellular mobility by blocking Akt activity, the stable HIP1-knockdown CL1-0 cells were treated with an Akt inhibitor, and transient overexpression of constitutively active myr-Akt was induced in stable HIP1-overexpressing CL1-5 cells (Figures 5C and 5D). The WB, migration and invasion assays showed that the CL1-0 shHIP1#1 and #2 cells treated with the Akt inhibitor showed increased levels E-cadherin, but decreases in pAkt-Thr308, pAkt-Ser473, pGSK3 $\beta$ -Ser9, Slug, Vimentin, and low cellular mobility. In contrast, the CL1-5 HIP1 cells transiently overexpressing myr-Akt had reduced E-cadherin, but more pAkt-Thr308, pAkt-Ser473, Akt, pGSK3 $\beta$ -Ser9, Slug, Vimentin, and high cellular mobility. These results suggest that the Akt-GSK3 $\beta$  signaling pathway mediates HIP1 inhibition of EMT.

To confirm that HIP1 regulated EMT and cellular mobility through  $\beta$ -catenin,  $\beta$ -catenin was transiently knocked-down in stable HIP1-knockdown CL1-0 cells, and transiently overexpressed in stable HIP1-overexpressing CL1-5 cells (Figures 5E and 5F). WB, migration and invasion assays showed that the CL1-0 shHIP1#1 and #2 cells with sh $\beta$ -catenin#1 and #2 respectively contained more E-cadherin, but less  $\beta$ -catenin, Slug, Vimentin, and low cellular mobility.  $\beta$ -catenin overexpression in the

CL1-5 HIP1 cells produced the opposite results. These results showed that HIP1 inhibited EMT through  $\beta$ -catenin. Collectively, our results suggest that HIP1 represses Akt activity to decrease the nuclear translocation of  $\beta$ -catenin and thereby blocks EMT.

**HIP1 restrains Akt in the cytoplasm to prevent its activation on the plasma membrane.**

To investigate the molecular mechanism by which HIP1 inhibited Akt activity, upstream regulatory molecules involved in the Akt activation were examined (Figure 6A). WB data showed that the levels of pAkt-Thr308 were increased in the CL1-0 shHIP1#1 and #2 cells, but were decreased in the CL1-5 HIP1 cells. The levels of Akt, phosphoinositide 3-kinase (PI3K) p85, and pPI3K p85-Tyr458 were not affected. These results revealed that HIP1 is not likely to affect Akt activation on the plasma membrane. To study the relationship between HIP1 and Akt, coimmunoprecipitation (co-IP) was performed. The data showed that HIP1 interacted with Akt in the HIP1-overexpressing CL1-5 cells (Figure 6B). Next, Akt was activated in starved CL1-5 cells by addition of 10% fetal bovine serum (FBS), and ICC/IF staining (Figure 6C) showed that the CL1-5 HIP1 cells had diminished levels of pAkt-S473 on the plasma membrane compared to control cells. These results suggest that HIP1

interaction with Akt restrains Akt in the cytoplasm and prevents its activation on the plasma membrane.

In order to evaluate downstream effects of HIP1-mediated reductions in Akt signaling, post-translational modifications of Slug were examined. Previous studies have reported that Slug is phosphorylated by GSK3 $\beta$  and then subsequently ubiquitinated by the carboxyl terminus of Hsc70-interacting protein (CHIP) for the Ubiquitin-proteasomal degradation (33, 34). We treated the HIP1-modified CL1 cells with MG132 (10  $\mu$ M) for 5 h (Figure 6D), and WB analysis showed that the CL1-0 Scramble and CL1-5 HIP1 cells had more Slug proteins compared to controls. These results suggest that HIP1 promoted the proteasomal degradation of Slug. Based on our findings that HIP1 promoted GSK3 $\beta$  activation, we suspect that HIP1 regulation of GSK3 $\beta$  is responsible for alterations in Slug phosphorylation and subsequent proteasomal degradation.

In conclusion, our findings (Figure 6E) show that HIP1 acts as a metastatic suppressor in NSCLC by inhibiting Akt-mediated EMT. Moreover, our data suggest that HIP1 interacts with Akt to decrease its activity, and inactive Akt does not phosphorylate and deactivate GSK3 $\beta$ . Elevated levels of active GSK3 $\beta$  suppress the nuclear translocation of  $\beta$ -catenin to reduce TCF4 activity, and diminish Slug expression. Eventually, the reduced level of Slug leads to Vimentin downregulation

and the E-cadherin upregulation, thus blocking EMT and preventing NSCLC metastasis.

## **Discussion**

NSCLC is the most common lung cancer, and its poor survival is mainly due to metastasis. Therefore, it is extremely important to understand the molecular mechanisms that drive metastasis in lung cancer biology, and to identify prognostic biomarkers in early-stage NSCLC. Although HIP1 was cloned (10, 11) and reported to associate with cancer in 1997-1998 (22), the precise role of HIP1 in tumor progression has remained unknown until now. Our study is the first to describe HIP1 involvement in AdCA metastasis. We found that HIP1 expression was reduced during metastasis-associated AdCA progression and acted as a metastatic suppressor in AdCA cells. Furthermore, we showed that HIP1 suppressed metastasis through modulation of the Akt-mediated EMT signaling pathway. Because current TNM staging does not provide satisfactory prognostication of the AdCA patients, it is essential to identify novel prognostic biomarkers of early stage AdCA. Our clinical analysis revealed that HIP1 was a prognostic biomarker in early-stage AdCA. Low HIP1 expression was highly predictive of poor patient survival.

In our study, we found that reductions in HIP1 expression promoted EMT

through the activation of Akt (Figures 4-6). Recently, numerous papers have shown that activation of the PI3K/Akt axis is a central feature of EMT, and may confer the cellular motility required for metastasis (35, 36). Our microarray data support this idea and show that HIP1 influenced several factors involved in metastatic regulation, including gene products associated with cytoskeletal and ECM remodeling. Cell mobility requires dynamically and spatially regulated changes in the actin cytoskeleton, microtubules, adhesion molecules and ECM (37). Accumulating evidence has also revealed that several key components closely associated with cytoskeletal dynamics are activated via Akt-mediated phosphorylation. In addition, Akt also interacts with other promigratory proteins, thus mediating crosstalk between affiliated signaling axes (38). Our results implicate HIP1 as a critical modulator of Akt-mediated EMT and associated cell motility in AdCA metastasis. In SCC, our results show similar phenomena that HIP1 down-regulation also enhances cell motility; however, there is no significance between knockdown and control groups (Figures E9 and E10).

According to clinical studies, the 5-year survival rate of patients with advanced NSCLC is less than 10%, whereas it is greater than 70% for patients with stage I disease. These statistics imply that the identification of prognostic biomarkers for early-stage AdCA has a meaningful clinical application (39, 40). In our Kaplan-Meier

log-rank analysis (Figures 1E and 1F), HIP1 expression during AdCA early stages were significantly correlated with patient's survival rates. The downregulation of HIP1 expression in early stage AdCA promoted metastasis and a poor prognosis. Thus, HIP1 represents a new prognostic biomarker for early-stage AdCA, and its application may bolster successful predictions of clinical outcomes in AdCA patients.

## **Acknowledgements**

The authors thank Dr. Yung-Ming Jeng for providing the clinical samples. The authors thank the Proteomics Core Facility and the Immunobiology Core Facility of the Clinical Medicine Research Center of National Cheng Kung University Hospital for assisting with the protein processing experiments and the fluorescence-activated cell sorting. Bioinformatic analyses were performed using the system provided by the Bioinformatics Core at the National Cheng Kung University, supported by the National Science Council, Taiwan. RNAi reagents were obtained from the National RNAi Core Facility Platform located at the Institute of Molecular Biology/ Genomic Research Center, Academia Sinica, supported by the National Core Facility Program for Biotechnology Grants of NSC.

## References

1. Jemal A, Siegel R, Ward E, Hao Y, Xu J, Thun MJ. Cancer statistics, 2009. *CA: a cancer journal for clinicians* 2009; 59: 225-249.
2. Herbst RS, Heymach JV, Lippman SM. Lung cancer. *The New England journal of medicine* 2008; 359: 1367-1380.
3. Socinski MA, Crowell R, Hensing TE, Langer CJ, Lilenbaum R, Sandler AB, Morris D. Treatment of non-small cell lung cancer, stage IV: ACCP evidence-based clinical practice guidelines (2nd edition). *Chest* 2007; 132: 277S-289S.
4. Azzoli CG, Baker S, Jr., Temin S, Pao W, Aliff T, Brahmer J, Johnson DH, Laskin JL, Masters G, Milton D, Nordquist L, Pfister DG, Piantadosi S, Schiller JH, Smith R, Smith TJ, Strawn JR, Trent D, Giaccone G. American Society of Clinical Oncology Clinical Practice Guideline update on chemotherapy for stage IV non-small-cell lung cancer. *Journal of clinical oncology : official journal of the American Society of Clinical Oncology* 2009; 27: 6251-6266.
5. Felip E, Gridelli C, Baas P, Rosell R, Stahel R. Metastatic non-small-cell lung cancer: consensus on pathology and molecular tests, first-line, second-line, and third-line therapy: 1st ESMO Consensus Conference in Lung Cancer;

- Lugano 2010. *Annals of oncology : official journal of the European Society for Medical Oncology / ESMO* 2011; 22: 1507-1519.
6. van Klaveren RJ. Lung cancer screening. *Eur J Cancer* 2011; 47 Suppl 3: S147-155.
  7. Steeg PS. Tumor metastasis: mechanistic insights and clinical challenges. *Nature medicine* 2006; 12: 895-904.
  8. Quail DF, Joyce JA. Microenvironmental regulation of tumor progression and metastasis. *Nature medicine* 2013; 19: 1423-1437.
  9. Wan L, Pantel K, Kang Y. Tumor metastasis: moving new biological insights into the clinic. *Nature medicine* 2013; 19: 1450-1464.
  10. Kalchman MA, Koide HB, McCutcheon K, Graham RK, Nichol K, Nishiyama K, Kazemi-Esfarjani P, Lynn FC, Wellington C, Metzler M, Goldberg YP, Kanazawa I, Gietz RD, Hayden MR. HIP1, a human homologue of *S. cerevisiae* Sla2p, interacts with membrane-associated huntingtin in the brain. *Nature genetics* 1997; 16: 44-53.
  11. Wanker EE, Rovira C, Scherzinger E, Hasenbank R, Walter S, Tait D, Colicelli J, Lehrach H. HIP-I: a huntingtin interacting protein isolated by the yeast two-hybrid system. *Human molecular genetics* 1997; 6: 487-495.
  12. Holtzman DA, Yang S, Drubin DG. Synthetic-lethal interactions identify two

- novel genes, SLA1 and SLA2, that control membrane cytoskeleton assembly in *Saccharomyces cerevisiae*. *The Journal of cell biology* 1993; 122: 635-644.
13. Wesp A, Hicke L, Palecek J, Lombardi R, Aust T, Munn AL, Riezman H. End4p/Sla2p interacts with actin-associated proteins for endocytosis in *Saccharomyces cerevisiae*. *Molecular biology of the cell* 1997; 8: 2291-2306.
14. Engqvist-Goldstein AE, Kessels MM, Chopra VS, Hayden MR, Drubin DG. An actin-binding protein of the Sla2/Huntingtin interacting protein 1 family is a novel component of clathrin-coated pits and vesicles. *The Journal of cell biology* 1999; 147: 1503-1518.
15. Engqvist-Goldstein AE, Warren RA, Kessels MM, Keen JH, Heuser J, Drubin DG. The actin-binding protein Hip1R associates with clathrin during early stages of endocytosis and promotes clathrin assembly in vitro. *The Journal of cell biology* 2001; 154: 1209-1223.
16. Waelter S, Scherzinger E, Hasenbank R, Nordhoff E, Lurz R, Goehler H, Gauss C, Sathasivam K, Bates GP, Lehrach H, Wanker EE. The huntingtin interacting protein HIP1 is a clathrin and alpha-adaptin-binding protein involved in receptor-mediated endocytosis. *Human molecular genetics* 2001; 10: 1807-1817.
17. Metzler M, Legendre-Guillemain V, Gan L, Chopra V, Kwok A, McPherson PS,

- Hayden MR. HIP1 functions in clathrin-mediated endocytosis through binding to clathrin and adaptor protein 2. *The Journal of biological chemistry* 2001; 276: 39271-39276.
18. Rao DS, Chang JC, Kumar PD, Mizukami I, Smithson GM, Bradley SV, Parlow AF, Ross TS. Huntingtin interacting protein 1 Is a clathrin coat binding protein required for differentiation of late spermatogenic progenitors. *Molecular and cellular biology* 2001; 21: 7796-7806.
19. Mishra SK, Agostinelli NR, Brett TJ, Mizukami I, Ross TS, Traub LM. Clathrin- and AP-2-binding sites in HIP1 uncover a general assembly role for endocytic accessory proteins. *The Journal of biological chemistry* 2001; 276: 46230-46236.
20. Gottfried I, Ehrlich M, Ashery U. HIP1 exhibits an early recruitment and a late stage function in the maturation of coated pits. *Cellular and molecular life sciences : CMLS* 2009; 66: 2897-2911.
21. Hyun TS, Ross TS. HIP1: trafficking roles and regulation of tumorigenesis. *Trends in molecular medicine* 2004; 10: 194-199.
22. Ross TS, Bernard OA, Berger R, Gilliland DG. Fusion of Huntingtin interacting protein 1 to platelet-derived growth factor beta receptor (PDGFbetaR) in chronic myelomonocytic leukemia with t(5;7)(q33;q11.2). *Blood* 1998; 91:

4419-4426.

23. Ross TS, Gilliland DG. Transforming properties of the Huntingtin interacting protein 1/ platelet-derived growth factor beta receptor fusion protein. *The Journal of biological chemistry* 1999; 274: 22328-22336.
24. Bradley SV, Holland EC, Liu GY, Thomas D, Hyun TS, Ross TS. Huntingtin interacting protein 1 is a novel brain tumor marker that associates with epidermal growth factor receptor. *Cancer research* 2007; 67: 3609-3615.
25. Rao DS, Bradley SV, Kumar PD, Hyun TS, Saint-Dic D, Oravec-Wilson K, Kleer CG, Ross TS. Altered receptor trafficking in Huntingtin Interacting Protein 1-transformed cells. *Cancer cell* 2003; 3: 471-482.
26. Rao DS, Hyun TS, Kumar PD, Mizukami IF, Rubin MA, Lucas PC, Sanda MG, Ross TS. Huntingtin-interacting protein 1 is overexpressed in prostate and colon cancer and is critical for cellular survival. *The Journal of clinical investigation* 2002; 110: 351-360.
27. Bradley SV, Smith MR, Hyun TS, Lucas PC, Li L, Antonuk D, Joshi I, Jin F, Ross TS. Aberrant Huntingtin interacting protein 1 in lymphoid malignancies. *Cancer research* 2007; 67: 8923-8931.
28. Bradley SV, Oravec-Wilson KI, Bougeard G, Mizukami I, Li L, Munaco AJ, Sreekumar A, Corradetti MN, Chinnaiyan AM, Sanda MG, Ross TS. Serum

- antibodies to huntingtin interacting protein-1: a new blood test for prostate cancer. *Cancer research* 2005; 65: 4126-4133.
29. Lee JM, Dedhar S, Kalluri R, Thompson EW. The epithelial-mesenchymal transition: new insights in signaling, development, and disease. *The Journal of cell biology* 2006; 172: 973-981.
30. De Craene B, Berx G. Regulatory networks defining EMT during cancer initiation and progression. *Nature reviews Cancer* 2013; 13: 97-110.
31. Thiery JP. Epithelial-mesenchymal transitions in tumour progression. *Nature reviews Cancer* 2002; 2: 442-454.
32. Peinado H, Olmeda D, Cano A. Snail, Zeb and bHLH factors in tumour progression: an alliance against the epithelial phenotype? *Nature reviews Cancer* 2007; 7: 415-428.
33. Kao SH, Wang WL, Chen CY, Chang YL, Wu YY, Wang YT, Wang SP, Nesvizhskii AI, Chen YJ, Hong TM, Yang PC. GSK3beta controls epithelial-mesenchymal transition and tumor metastasis by CHIP-mediated degradation of Slug. *Oncogene* 2014; 33: 3172-3182.
34. Wang SP, Wang WL, Chang YL, Wu CT, Chao YC, Kao SH, Yuan A, Lin CW, Yang SC, Chan WK, Li KC, Hong TM, Yang PC. p53 controls cancer cell invasion by inducing the MDM2-mediated degradation of Slug. *Nat Cell Biol*

- 2009; 11: 694-704.
35. Grille SJ, Bellacosa A, Upson J, Klein-Szanto AJ, van Roy F, Lee-Kwon W, Donowitz M, Tsihchlis PN, Larue L. The protein kinase Akt induces epithelial mesenchymal transition and promotes enhanced motility and invasiveness of squamous cell carcinoma lines. *Cancer research* 2003; 63: 2172-2178.
36. Larue L, Bellacosa A. Epithelial-mesenchymal transition in development and cancer: role of phosphatidylinositol 3' kinase/AKT pathways. *Oncogene* 2005; 24: 7443-7454.
37. Xue G, Hemmings BA. PKB/Akt-dependent regulation of cell motility. *Journal of the National Cancer Institute* 2013; 105: 393-404.
38. Enomoto A, Murakami H, Asai N, Morone N, Watanabe T, Kawai K, Murakumo Y, Usukura J, Kaibuchi K, Takahashi M. Akt/PKB regulates actin organization and cell motility via Girdin/APE. *Developmental cell* 2005; 9: 389-402.
39. Hassanein M, Callison JC, Callaway-Lane C, Aldrich MC, Grogan EL, Massion PP. The state of molecular biomarkers for the early detection of lung cancer. *Cancer Prev Res (Phila)* 2012; 5: 992-1006.
40. Jiang F, Todd NW, Li R, Zhang H, Fang H, Stass SA. A panel of sputum-based genomic marker for early detection of lung cancer. *Cancer Prev Res (Phila)* 2010; 3: 1571-1578.

Table 1. The Cox Multivariate Regression Analysis of TNM Prognostic Factors and HIP1 Expressions for Overall and Disease-free Survival of 121 NSCLC Patients in the First Cohort

Overall Survival (OS)				
Variables	Comparison	Hazard Ratio (95% CI)	<i>p</i> -value	
T	T1-T2; T3-T4	1.321 (0.822-2.120)	0.250	
N	N0; N1-N3	1.964 (1.203-3.206)	0.007	**
M	M0; M1	1.803 (1.110-2.930)	0.017	*
HIP1	Low (0, 1); High (2, 3)	2.268 (1.421-3.619)	0.001	**
Disease-free Survival (DFS)				
Variables	Comparison	Hazard Ratio (95% CI)	<i>p</i> -value	
T	T1-T2; T3-T4	1.356 (0.840-2.188)	0.213	
N	N0; N1-N3	2.062 (1.276-3.333)	0.003	**
M	M0; M1	1.454 (0.891-2.373)	0.134	
HIP1	Low (0, 1); High (2, 3)	2.119 (1.354-3.316)	0.001	**

NOTE: Cox proportional hazards regression was used to test independent prognostic contribution of HIP1 after accounting for other potentially important covariates.

Abbreviations: HR, hazard ratio; CI, confidence interval

\* Two-sided Cox proportional hazards regression using normal approximation and  $p < 0.05$  was considered statistically significant.

Table 2. The Clinicopathologic Characteristics of 121 NSCLC Patients in the First Cohort with Low and High HIP1 expressions

Characteristic	Low Expression (score 0-1), n = 71	High Expression (score 2-3), n = 50	<i>p</i> Value
Age (mean ± SD) (in years)	60.24 ± 1.19	63.94 ± 1.45	0.05 <sup>a</sup> *
Sex, no. of patients			0.483 <sup>b</sup>
Male	38	30	
Female	33	20	
Stage, <sup>c</sup> no. of patients			0.040 <sup>b</sup> *
I-II	25	27	
III-IV	46	23	
Tumor status, <sup>c</sup> no. of patients			0.286 <sup>b</sup>
T1-T2	46	37	
T3-T4	25	13	
Lymph nodal status, <sup>c</sup> no. of patients			0.362 <sup>b</sup>
N0	24	21	
N1-N3	47	29	
Metastasis, <sup>c</sup> no. of patients			0.005 <sup>b</sup> **
M0	43	42	
M1	28	8	
Histology, no. of patients			0.112 <sup>b</sup>
Adenocarcinoma	38	34	
Nonadenocarcinoma	33	16	
Median survival (in months)	22	62	1.276E-5 <sup>d</sup> ***

<sup>a</sup> *p* value was measured with student's *t* test.

<sup>b</sup> *p* values were derived with Pearson chi-square tests.

<sup>c</sup> The tumor stage, tumor status, lymph node status, and metastasis were classified according to the international system for staging lung cancer.

<sup>d</sup> *p* values was derived with log rank test.

---

All statistical tests are two sided. SD, standard deviation.

---

### Figure legends

**Figure 1.** HIP1 expression is upregulated in NSCLC, and low HIP1 expression is correlated with poor prognosis in AdCA progression. (A) Representative HIP1 IHC staining in clinical specimens from four groups: normal, stage I, stage II/III and stage IV. (B) The percentage of low (score 0-1) and high (score 2-3) HIP1 expression levels were calculated in the four groups of NSCLC specimens. (C and D) Low-level HIP1 expression significantly correlated with poor overall and disease-free survival in NSCLC patients. (E and F) Low-level HIP1 expression during the early stages of NSCLC significantly correlated with poor survival. (G) The ratio of low/high HIP1 expression in patients with metastasis was significantly higher than in patients without metastasis.

**Figure 2.** HIP1 regulates the mobility of AdCA cells. (A) Endogenous HIP1 expression levels in the CL1 cell lines were analyzed using WB and RT-PCR.  $\alpha$ -tubulin and GAPDH were used as internal controls for the levels of protein and mRNA, respectively. (B) The migratory and invasion abilities of CL1-0, CL1-2,

CL1-3 and CL1-5 cells were evaluated using migration and invasion assays. (C) HIP1 expression levels and the growth of stably HIP1-modified CL1 cells were analyzed using WB and MTT assays. (D) The migratory abilities of stably HIP1-modified CL1 cells were evaluated using wound-healing assays. (E) The cellular mobility of stably HIP1-modified CL1 cells were evaluated using migration and invasion assays. (F) The cellular mobility of HIP1-re-manipulated CL1 cells were evaluated using migration and invasion assays.

**Figure 3.** HIP1 affects AdCA metastasis *in vivo*. (A) Orthotopic lung injection was performed to deliver HIP1-modified CL1 cells into mice. After the removed lungs were photographed and the metastatic tumor cells counted, tissues were paraffin-embedded and metastatic tumor cells were verified using HE stain. The yellow triangles and open rectangles indicate the injected lung adenocarcinoma in the left lungs of mice. The red triangles and open rectangles indicated the metastatic tumor cells in the right lungs of mice. (B) Tail vein injection was performed to deliver HIP1-modified CL1 cells into mice. The metastatic tumor cells were photographed, counted and verified using HE stain. The red triangles and black open rectangles indicated the metastatic tumor cells on the lung tissue sections. (C) The metastatic tumor cells were stained using IHC against human mitochondria in the CL1-5 groups

with tail vein injection. The red open rectangles indicated the metastatic tumor cells on the lung tissue sections.

**Figure 4.** HIP1 regulates EMT. (A) EMT-related genes in MetaCore were divided into two groups based on the microarray data, with red indicating upregulation and green indicating downregulation under HIP1-knockdown conditions. (B) Microarray data were analyzed using MetaCore bioinformatics software to identify the HIP1-regulated signaling pathways involved in EMT. (C) The endogenous expression levels of EMT markers in CL1 cells were detected using WB. (D) Under the TGF $\beta$ -induced EMT, the expressions of HIP1 and E-cadherin in A549 cells were detected using WB. (E) In the HIP1-knockdown CL1-0 cells, the expression levels of EMT-related genes were examined using qPCR and WB. (F) In the HIP1-overexpressing CL1-5 cells, the expression levels of EMT-related genes were examined using qPCR and WB. (G) The nuclear translocation of  $\beta$ -catenin was evaluated using nuclear and cytoplasmic extraction and WB. (H) TCF4 activity was measured using a luciferase reporter assay. GAPDH and  $\alpha$ -tubulin were used as internal controls of qPCR and WB, respectively. Lamin A/C and  $\alpha$ -tubulin were used as internal controls for WB in the nucleus and cytoplasm isolations, respectively.

**Figure 5.** HIP1 participates in Akt-mediated EMT. (A) The phosphorylated forms of GSK3 $\beta$ , Akt and PDK1 were evaluated in HIP1-modified CL1 cells using WB. (B) Molecules involved in Akt-mediated EMT were evaluated in HIP1-remanipulated CL1 cells using WB. (C) Akt activity was manipulated in HIP1-modified CL1 cells, after which, the levels of molecules involved in Akt-mediated EMT were evaluated using WB. (D) The cellular mobility of stably HIP1-modified CL1 cells with Akt manipulation was evaluated using migration and invasion assays. (E) The expression of  $\beta$ -catenin was manipulated in HIP1-modified CL1 cells, after which, the levels of molecules involved in EMT were evaluated using WB. (F) The cellular mobility of stably HIP1-modified CL1 cells with  $\beta$ -catenin manipulation were evaluated using migration and invasion assays.

**Figure 6.** HIP1 retains Akt in the cytoplasm inhibiting its activation on the plasma membrane. (A) The upstream regulatory molecules involved in the Akt activation were examined using WB.  $\alpha$ -tubulin was used as the internal control. (B) The interaction between HIP1 and Akt was detected using co-IP. (C) The cellular location of pAkt-S473 was probed using ICC/IF stain. pAkt-S473: green. Red triangles indicates the membrane localization of pAkt-S473. (D) The HIP1-modified CL1 cells were treated with MG132 (10  $\mu$ M) for 5 h, and the Slug expressions were detected

using WB.  $\alpha$ -tubulin was used as the internal control. (E) A schematic representation shows HIP1 regulation of the Akt-mediated EMT signaling pathway.

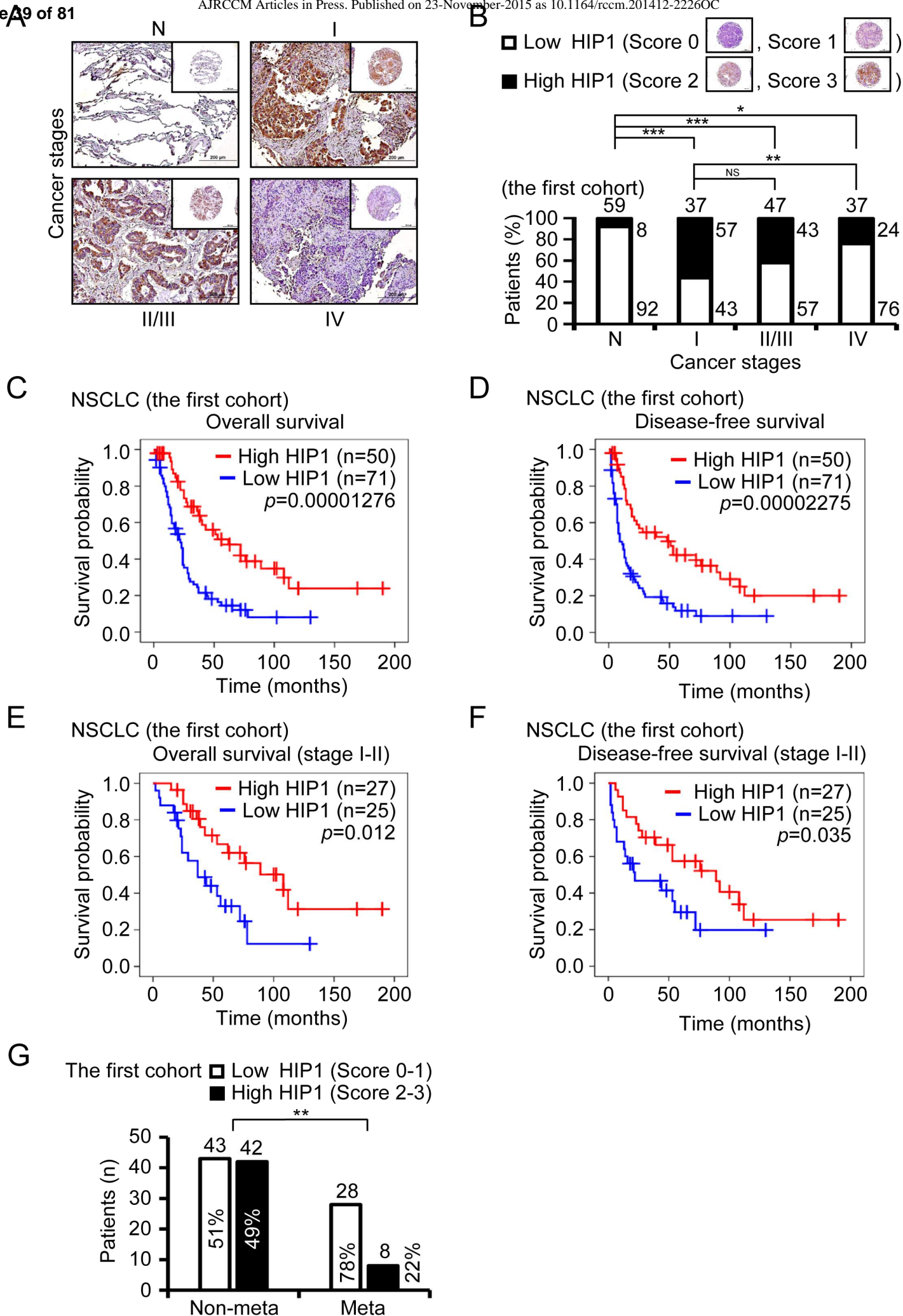
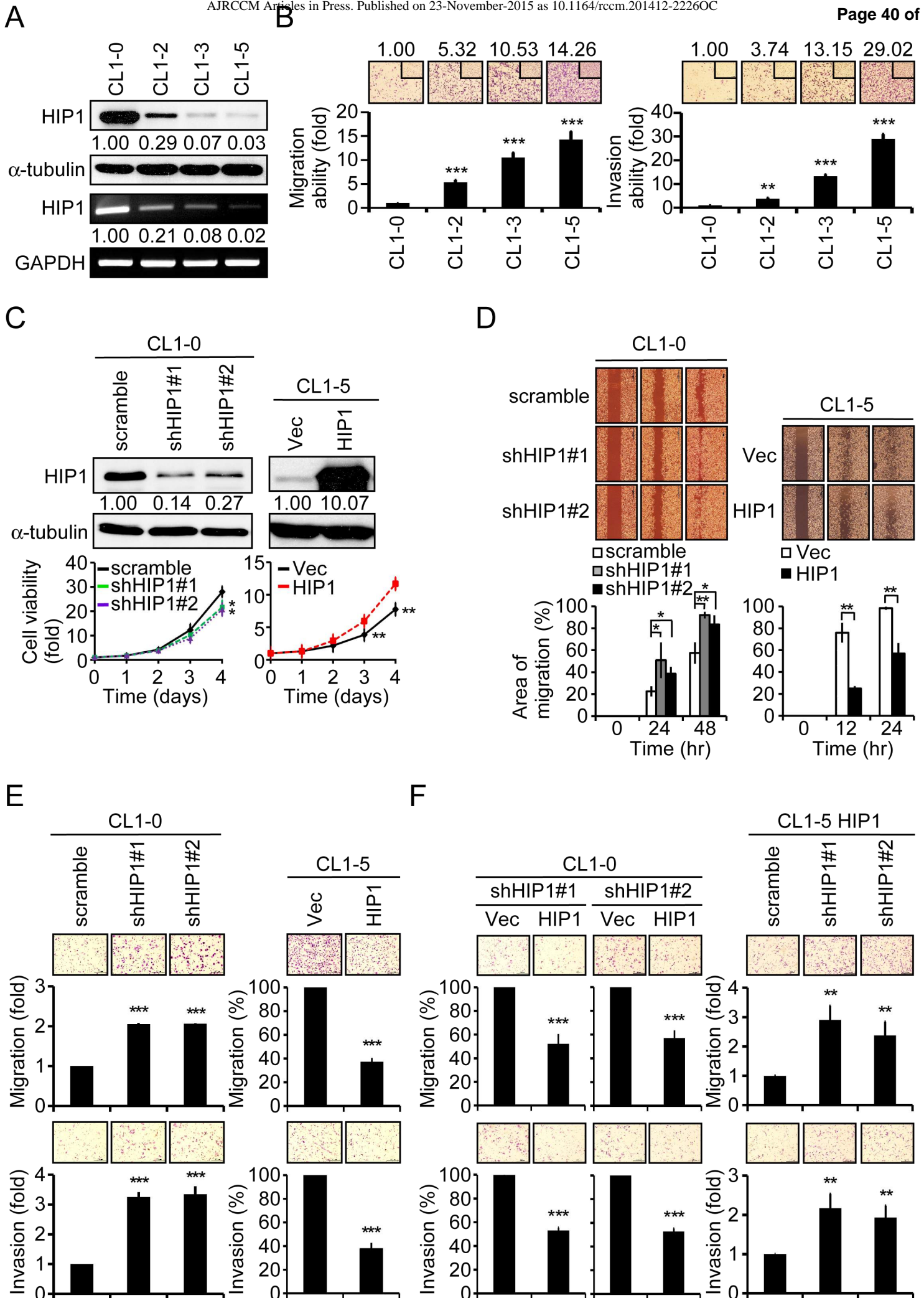


Figure 1 (Hsu et al.)



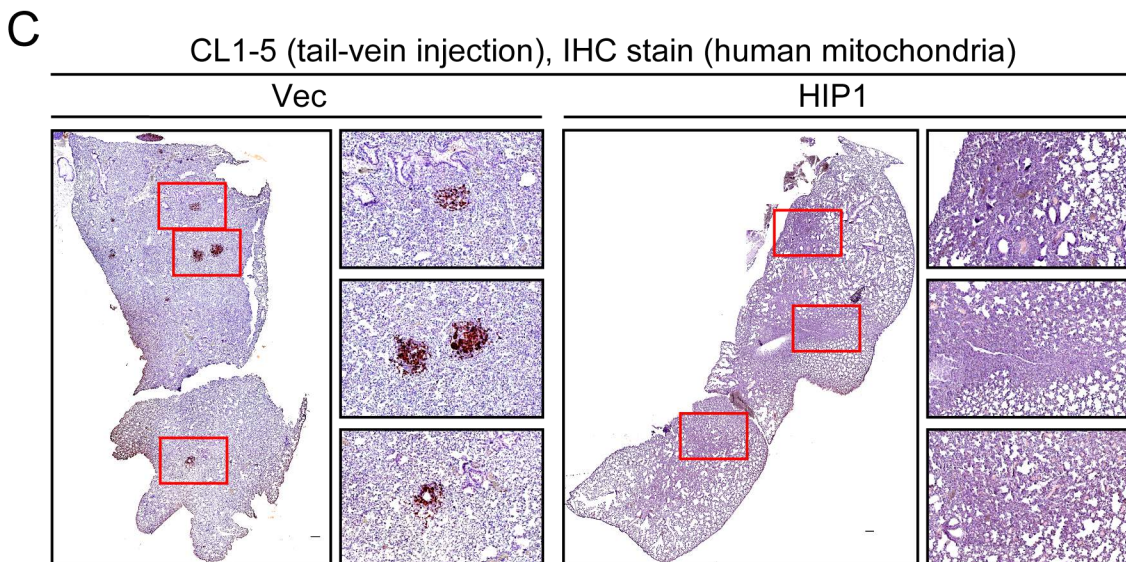
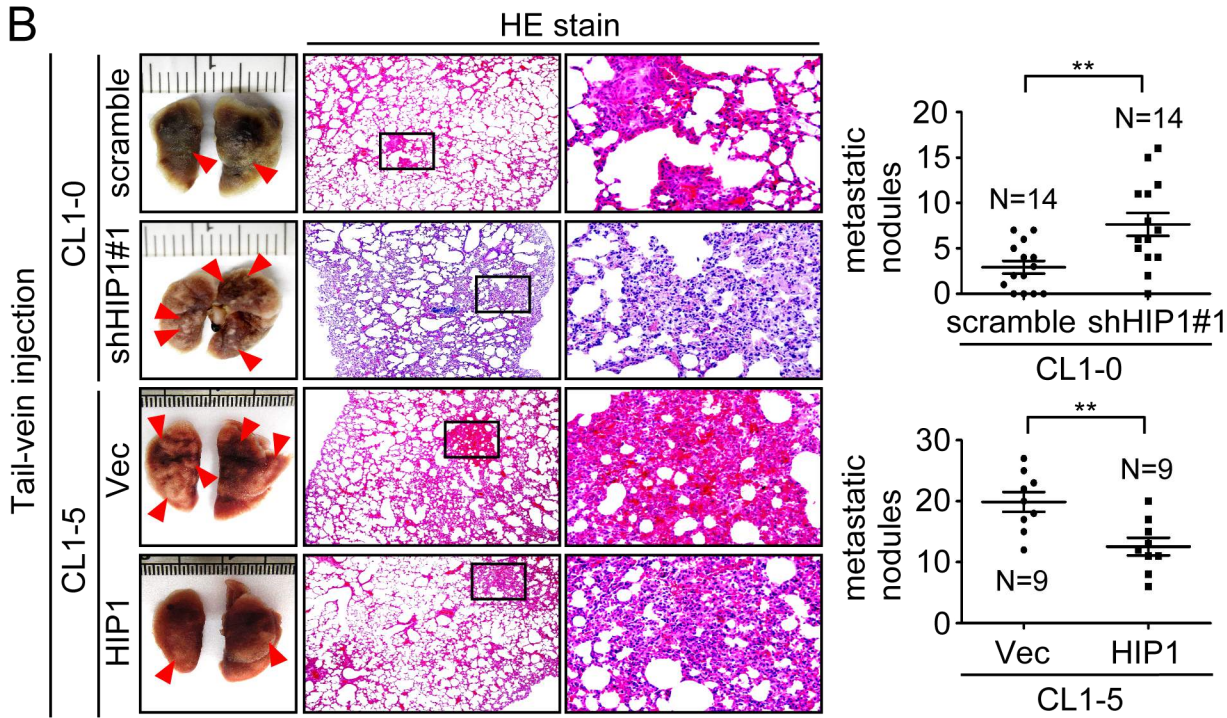
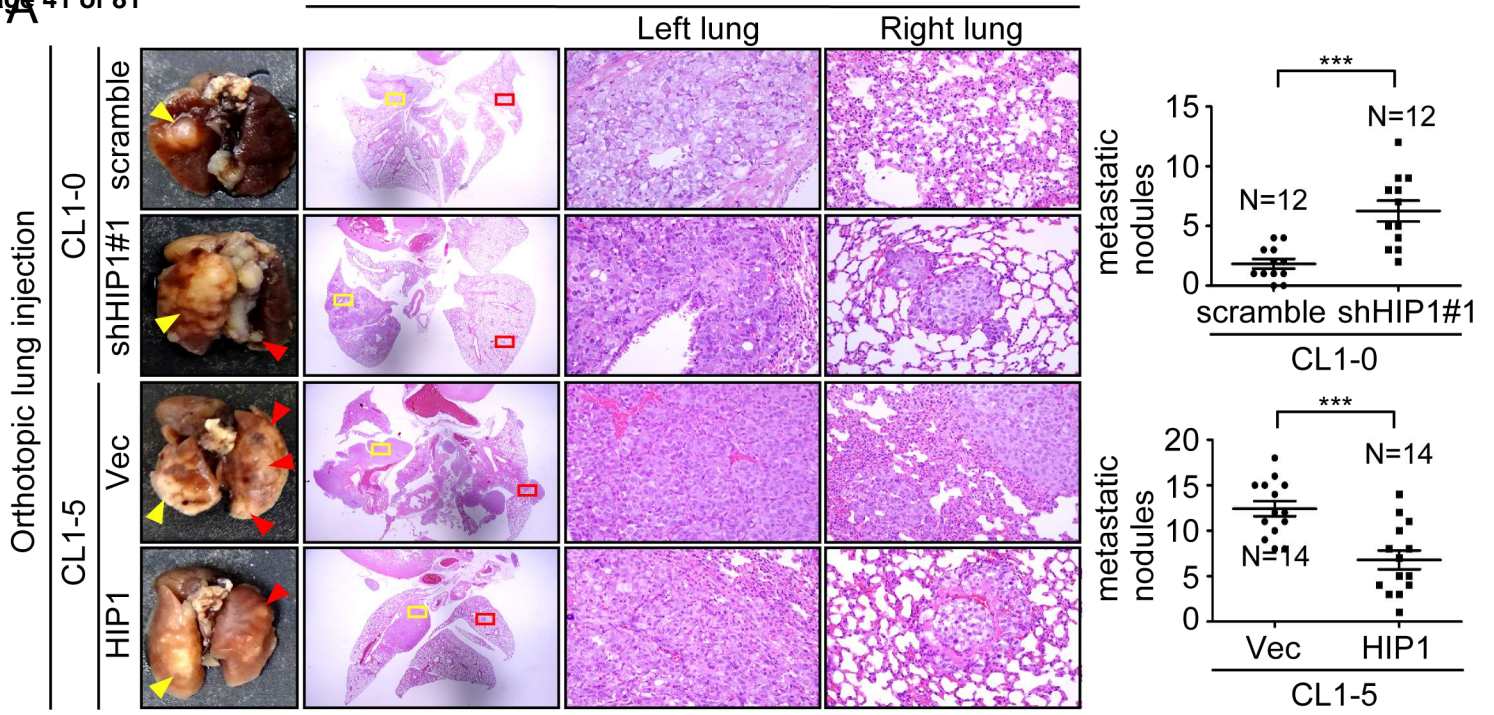
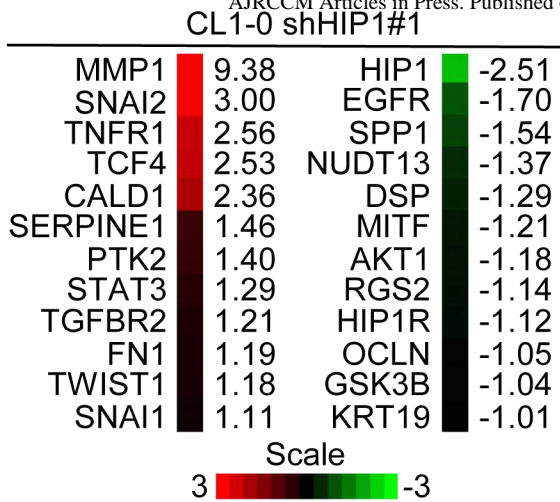


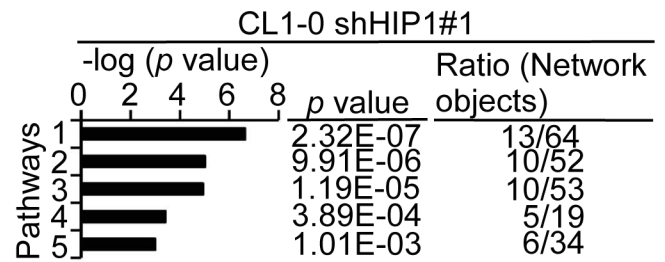
Figure 3 (Hsu et al.)

**A**

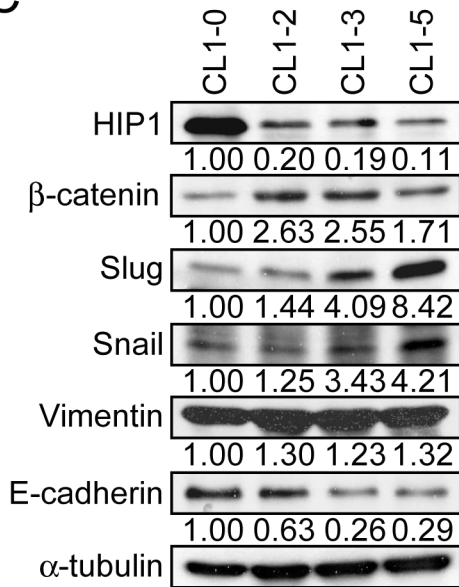


**B**

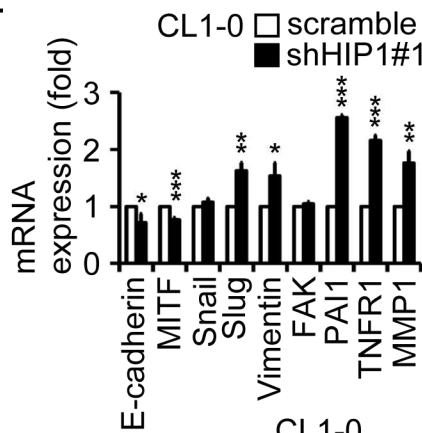
1. Regulation of epithelial-to-mesenchymal transition (EMT)
2. Cell adhesion\_ECM remodeling
3. WNT signaling pathway
4. NOTCH-induced EMT
5. HGF-dependent inhibition of TGFβ-induced EMT



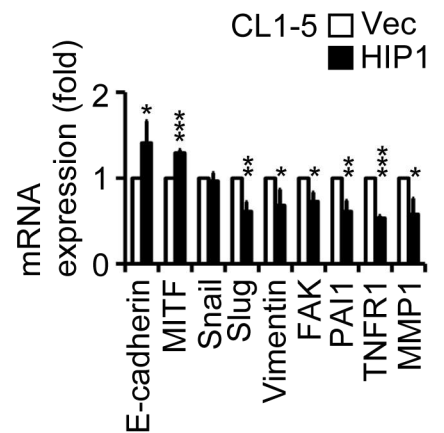
**C**



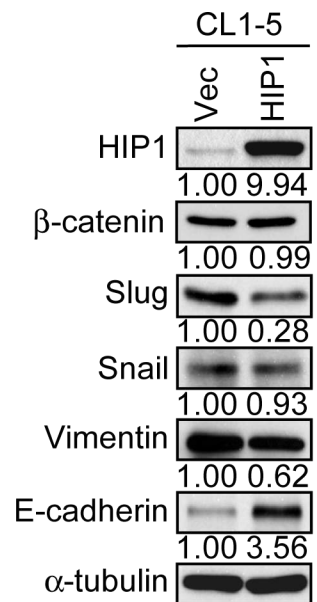
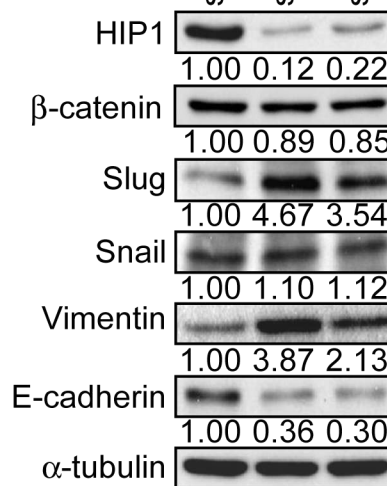
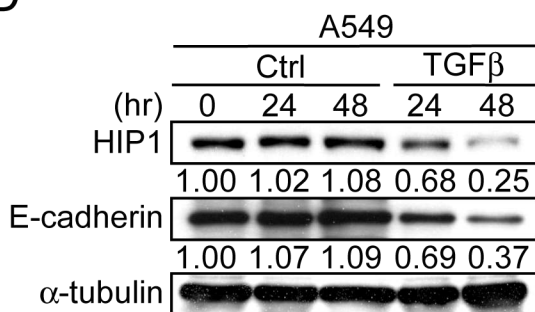
**E**



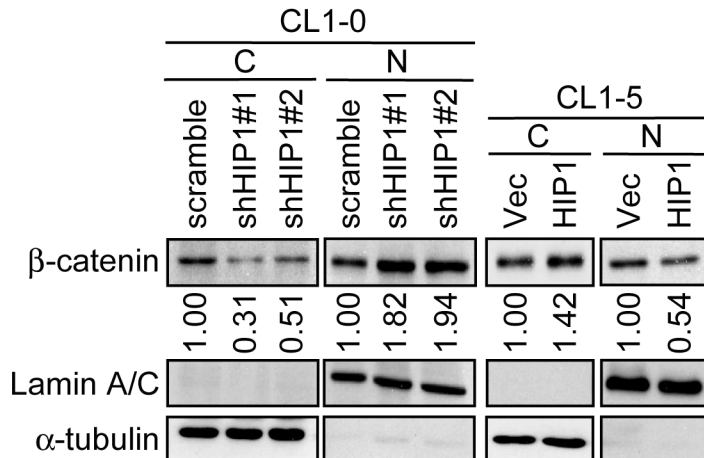
**F**



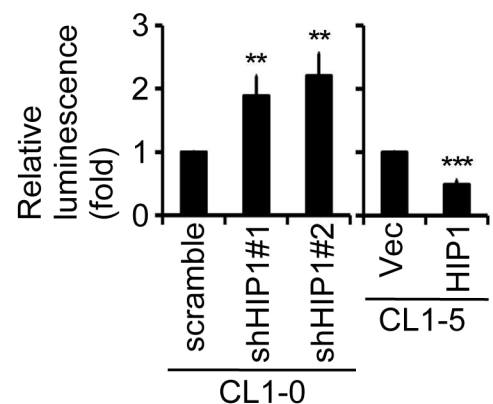
**D**



**G**



**H**



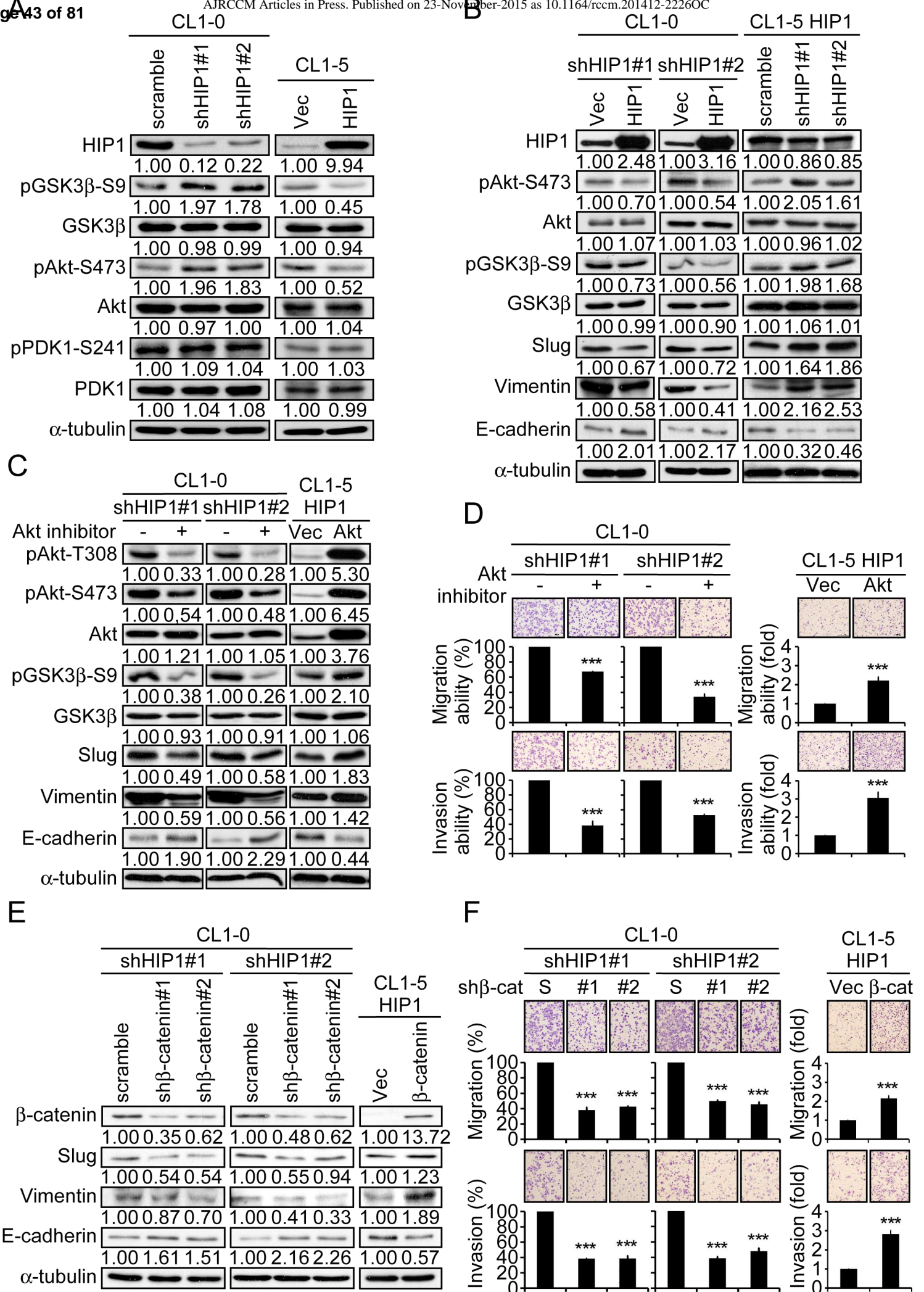
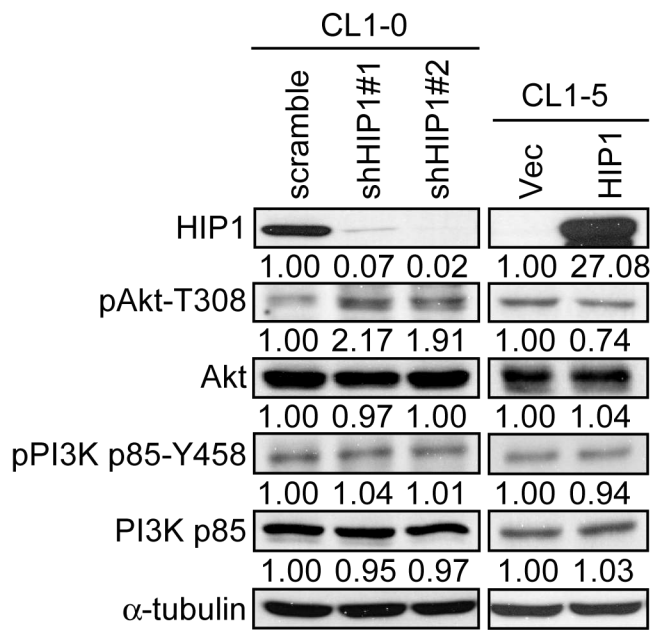
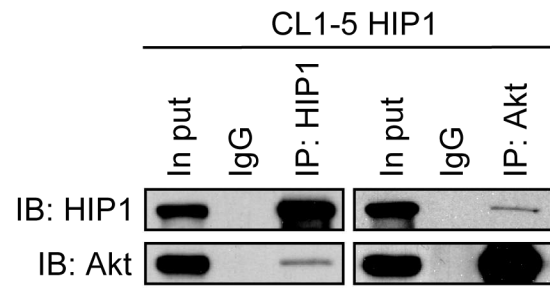


Figure 5 (Hsu et al.)

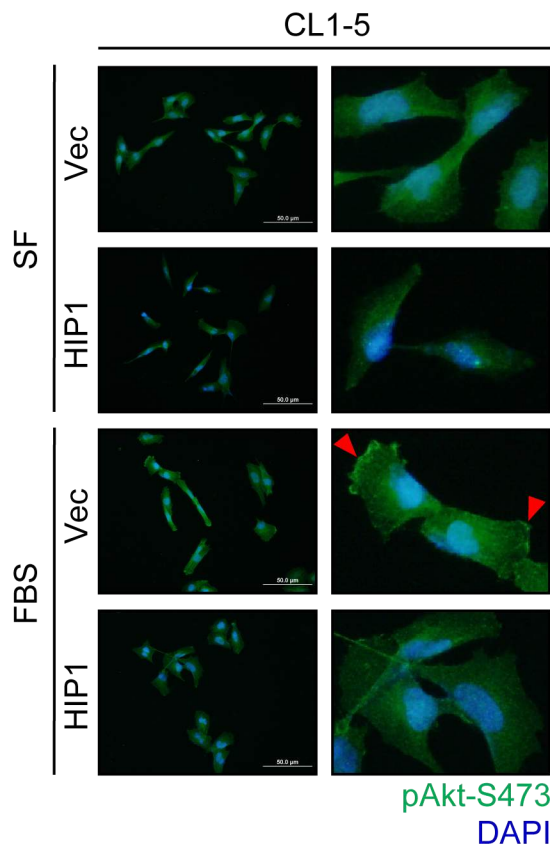
A



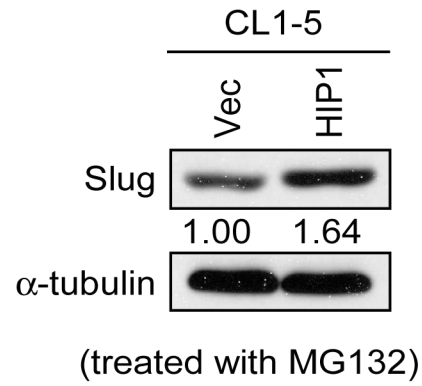
B



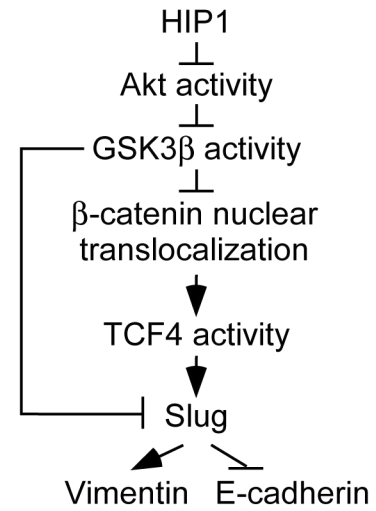
C



D



E



## Supplemental Information

### **HIP1 is an Early-Stage Prognostic Biomarker of Lung Adenocarcinoma and Suppresses Metastasis via Akt-mediated EMT**

Che-Yu Hsu<sup>1#</sup>, Cheng-Han Lin<sup>2,3#</sup>, Yi-Hua Jan<sup>3</sup>, Chia-Yi Su<sup>3</sup>, Yun-Chin Yao<sup>4</sup>,  
Hui-Chuan Cheng<sup>2</sup>, Tai-I Hsu<sup>1</sup>, Po-Shun Wang<sup>2</sup>, Wen-Pin Su<sup>2</sup>, Chih-Jen Yang<sup>5</sup>,  
Ming-Shyan Huang<sup>5</sup>, Marcus J Calkins<sup>2</sup>, Michael Hsiao<sup>3\*</sup>, and Pei-Jung Lu<sup>1,2\*</sup>

\* Correspondence should be addressed to:

pjlu2190@mail.ncku.edu.tw

mhsiao@gate.sinica.edu.tw

#### Inventory of all Supplemental Information

Supplemental materials and methods

Supplementary figure legends

Supplementary tables: Table E1

Supplemental figures: Figure E1, E2, E3, E4, E5, E6, E7, E8, E9, E10

#### **Supplementary materials and methods**

### **Cell culture, animal model and reagents**

The CL1-0, CL1-2, CL1-3, CL1-5, PC9, PC13, H441, H661 and H928 cell lines were cultured in RPMI medium 1640 (GIBCO, Gaithersburg, MD) supplemented with 10% fetal bovine serum (FBS) and 1% antibiotics (penicillin-streptomycin solution) (HyClone, Logan, UT). The A549, H1299 and HEK293T cell lines were cultured in Dulbecco's modified Eagle's medium (DMEM, GIBCO) supplemented with 10% FBS and 1% antibiotics. All cell cultures were maintained in a 5% CO<sub>2</sub> humidified atmosphere at 37°C. In the case of long-term culturing, a mycoplasma test of each cell line was conducted monthly. The CL1 cell lines were kindly supplied by Dr Pan-Chyr Yang (National Taiwan University, Taipei, Taiwan), and others were obtained from ATCC (Manassas, VA).

### **Orthotopic and tail vein injections**

Nude mice (8-week-old males, with a body weight of 20-25 g) were obtained from the National Laboratory Animal Center. Animal care was provided in accordance with the Laboratory Animal Welfare Act and the Guide for the Care and Use of Laboratory Animals and was approved by the Institutional Animal Care and Use Committee of National Cheng Kung University. The animal experiments were conducted by injecting nude mice orthotopically and via the tail vein with stably

HIP1-modified CL1 cells. For the orthotopic (lung) injections, the left lung of each mouse was inoculated with  $1 \times 10^5$  HIP1-modified cells in 10  $\mu$ l of Hank's balanced salt solution (HBSS, GIBCO) containing 50% Matrigel (BD Biosciences, San Jose, CA). For the tail vein injections,  $1 \times 10^6$  HIP1-modified cells were suspended in 100  $\mu$ L of HBSS and injected into the lateral tail veins of nude mice. The mice injected with HIP1-knockdown CL1-0 and HIP1-overexpressing CL1-5 cells were sacrificed at 8 and 5 weeks post-injection. The lungs were removed and fixed using 10% formalin, and the tumor nodules were counted under a dissecting microscope the following day. Among the orthotopically injected mice, metastatic nodules in the right lungs were counted. The metastatic nodules were counted in both lungs of mice with the tail vein injections. Finally, the metastatic tumor nodules were verified using hematoxylin and eosin (HE) stain.

### **Akt inhibition**

Akt activity was inhibited by treatment with 1  $\mu$ M Akt inhibitor IV (SIGMA, St Louis, MO), and the cell lysates were collected at 24 h post-treatment. Under TGF $\beta$  (5 ng/ml) treatment (SIGMA), EMT were induced successfully in A549 cells. To inhibit the proteasomal degradation of Slug, the HIP1-modified CL1 cells were treated with MG132 (10  $\mu$ M, SIGMA) for 5 h.

### **Plasmid construction, DNA transfection and lentivirus transduction**

In the overexpression experiments, the pLEX-MCS\_HIP1-fCDS construct for the expression of full-length cDNA of human HIP1 (NM\_005338) was constructed using the lentiviral vector pLEX-MCS (Thermo Scientific, San Jose, CA), the pCMV-myr-Akt construct for the expression of constitutively active myr-Akt was constructed using the pCMV vector, and the pEGFPC1- $\beta$ -catenin construct for the expression of full-length cDNA of human  $\beta$ -catenin (NM\_001904) was constructed using the vector pEGFPC1. In the knockdown experiments, the lentiviral plasmids (Thermo Scientific) containing the pGIPZ non-silencing shRNA control, pGIPZ-shHIP1#1 (V3LHS\_341239) and pGIPZ-shHIP1#2 (V3LHS\_341243) were used to knockdown HIP1 expressions. The lentiviral plasmids (NRC, Academia Sinica, Taiwan) containing the pLKO.1 non-silencing shRNA control, pLKO.1-sh $\beta$ -catenin#1 (TRCN0000003845) and pLKO.1-sh $\beta$ -catenin#2 (TRCN0000350477) were used to knockdown  $\beta$ -catenin expressions.

DNA transfection was performed using 50% confluent cells in 6-cm culture dishes. For transient transfection, 4  $\mu$ g of plasmid DNA and 10  $\mu$ l of Lipofectamine 2000 (Invitrogen, Carlsbad, CA) were each diluted with 500  $\mu$ l of Opti-MEM (GIBCO) and incubated at room temperature for 5 min. The diluted DNA and

Lipofectamine 2000 solutions were mixed gently and incubated for 20 min. Finally, 1 ml of the mixture was added into each 6-cm dish containing cells and 2 ml of serum-free medium, and the cells were cultured at 37°C in 5% CO<sub>2</sub> for 6 h. The culture medium was renewed to terminate the transfection, and cells were kept in the incubator for subsequent experiments.

Stably HIP1-modified cells were generated by transduction using lentiviral particles carrying pLEX-MCS/pLEX-MCS\_HIP1-fCDS and the pGIPZ non-silencing shRNA control/pGIPZ-shHIP1#1, #2. For the lentivirus preparations, 2x10<sup>6</sup> HEK293T cells were seeded in a 10-cm culture dish. Using a standard calcium phosphate transfection protocol, 9 µg of the transfer plasmids, 6 µg of psPAX2 and 3 µg of pMD2.G were co-transfected into HEK293T cells. The culture medium was renewed 6 h later, and the virus-containing supernatants were collected at 48 h post-transfection. Lentiviral infection was performed by adding virus-containing medium to cells and culturing them overnight. Stably transduced cells were selected using puromycin (SIGMA), and heterogeneous pools of fluorescent clones were sorted using fluorescence-activated cell sorting (FACS).

### **RT-PCR, quantitative real-time PCR (qPCR) and microarray analysis**

Total RNAs were isolated using TRIzol (Invitrogen) according to the

manufacturer's instructions. cDNAs were produced from 1 µg of isolated RNAs using M-MLV reverse transcriptase (Invitrogen), and the reverse transcription reaction was performed under the following conditions: 42°C for 1 h, 70°C for 15 min and 4°C for 5 min. The PCR protocol was conducted as follows: one cycle at 95°C for 3 min, followed by 25 cycles of 30 seconds at 95°C, 30 seconds at 60°C and 30 seconds at 72°C, with a final extension at 72°C for 10 min. The PCR products were detected by 2% agarose gel electrophoresis.

The qPCR was performed using Fast SYBR<sup>®</sup> Green Master Mix (Abcam, Cambridge, MA) under the following conditions: one cycle at 95°C for 20 seconds, followed by 40 cycles of denaturation at 95°C for 3 seconds and annealing at 60°C for 30 seconds. The RNA levels detected using RT-PCR and qPCR were consequently normalized against the level of human glyceraldehyde-3-phosphate dehydrogenase (GAPDH).

For the microarray analysis, total RNAs of stable CL1-0 Scramble and shHIP1#1 cells were prepared using an RNeasy Mini Kit (QIAGEN, Valencia, CA). The synthesis and fragmentation of the labeled aRNAs were performed using a GeneChip<sup>®</sup> 3' IVT Express Kit (Affymetrix, Santa Clara, CA). Target hybridization was conducted using a Human Genome U133 Plus 2.0 GeneChip<sup>®</sup>. The signals were detected using a GeneChip<sup>®</sup> Scanner 3000 7G. The fold changes in the transcriptomic

analysis were determined using Agilent GeneSpring GX 11.5 software. MetaCore bioinformatics software was used to determine the categories of genes with altered expression levels (significant differences as  $\log_2$  (fold changes) at  $> 0.5$ ).

### **Western blotting (WB), subcellular fractionation analysis and coimmunoprecipitation (co-IP)**

Before conducting WB, the cells were lysed using RIPA buffer (Millipore, Billerica, MA) containing proteinase and phosphatase inhibitors. The protein concentrations were determined using a Bio-Rad Protein Assay Dye Reagent Concentrate (Bio-Rad, Hercules, CA). For WB, an aliquot of 20-30  $\mu\text{g}$  of total protein that was boiled in 2x sample loading buffer (0.1 M Tris-HCl at pH 6.8, 4% SDS, 20% glycerol, 2%  $\beta$ -mercaptoethanol and a small amount of Bromophenol blue) was loaded onto a 7.5-15% SDS-polyacrylamide gel for electrophoresis (SDS-PAGE) at 80-100 V and then transferred to a PVDF membrane (Millipore) at 100 V for 1.5 h. The proteins-coated membranes were blocked with 5% non-fat milk in TBST (Tris Buffered Saline with Tween 20) overnight. The candidate proteins were identified by incubating the membranes with primary antibodies at room temperature for 2 h, and then the membranes were washed in TBST four times for 1 h. After washing, the membranes were incubated with horseradish peroxidase (HRP)-conjugated secondary

antibodies at room temperature for 1 h. Finally, the membranes were washed again, and followed by an enhanced chemiluminescence solution (PerkinElmer, Waltham, MA) for signal detection.  $\alpha$ -tubulin was used as the internal control for normalization.

The cytoplasmic and nuclear extracts of mammalian cells were obtained using NE-PER<sup>®</sup> Nuclear and Cytoplasmic Extraction Reagents (Thermo Scientific). For the subcellular fractionation analysis,  $2 \times 10^6$  cells were collected and dissolved in 20  $\mu$ l of cold CER. Next, 11  $\mu$ l of cold CER II was added, and the supernatant was collected as the cytoplasmic extract. Then, 100  $\mu$ l of cold NER was added to the pellet, and the supernatant was collected as the nuclear extract. Finally, the cytoplasmic and nuclear extracts were used for WB with  $\alpha$ -tubulin and lamin A/C, respectively, as the internal controls.

For co-IP, the supernatants of the cellular lysates were pre-absorbed using beads (Protein A Agarose, Calbiochem, San Diego, CA; Protein G Agarose, Millipore) for 1 h at room temperature. Supernatants containing 1 mg of protein were transferred to new tubes containing 20  $\mu$ l of beads and 2  $\mu$ g of antibodies specific for the candidate proteins in a final volume of 500  $\mu$ l of co-IP binding buffer (0.1 M HEPES or Tris at pH 7.4, 0.15 M NaCl, 2 mM EDTA, 0.5% Tween-20 and 0.01% NP-40). Incubation was conducted with constant rocking at 4°C overnight, and then the beads were washed 3 times with cold co-IP binding buffer. Finally, the sample beads were

collected, resuspended in 2x sample loading buffer and boiled for 10 min for use in WB assays.

**Tissue-array, immunohistochemistry (IHC), hematoxylin/eosin stain (HE stain) and immunocytochemistry (ICC)/immunofluorescence (IF)**

In our studies, three cohorts were analyzed using IHC staining to visualize HIP1 expressions of clinical specimens. The first cohort covered two tissue arrays TA38A and TA38B, and these lung specimens were collected from the Kaohsiung Medical University Chung-Ho Memorial Hospital (KMUH, Kaohsiung, Taiwan). TA38AB included 19 xenografts and 121 non-small cell lung cancer (NSCLC) patients containing 72 adenocarcinomas (AdCAs), 40 squamous cell carcinomas (SCCs) and 9 large cell carcinomas (LCCs). The second cohort consisted of TA38AB and some lung tissue sections from National Taiwan University Hospital (NTUH) containing 79 NSCLC patients (48 AdCAs, 18 SCCs and 13 others). The third cohort was composed of two tissue arrays TACCA4 and TACC5, and these lung specimens from Korea contained 89 NSCLC patients (28 AdCAs, 48 SCCs and 13 others). The tissue-array chips and the clinical lung tissue sections were supplied by Dr. Michael Hsiao (Academia Sinica, Taipei, Taiwan). All clinical tissues were fixed using 10% formalin, dehydrated, paraffin-embedded and sectioned.

When IHC was performed, the slides were heated at 65°C for 2 h, and they were deparaffinized using xylene (3x10 min) and rehydrated using a graduated ethanol series (two repeats of 100, 95 and 75% for 5 min each). Antigen retrieval was performed by immersion in 0.1 M citrate buffer (pH 6.0) and boiling in a microwave oven for 20 min. The sections were blocked using normal horse or goat serum at room temperature for 30 min and then incubated with primary antibodies at 4°C overnight. Next, the sections were incubated with biotinylated secondary antibody and streptavidin-peroxidase reagent (Vector<sup>®</sup> Blue Alkaline Phosphatase Substrate Kit, Vector, Burlingame, CA) at room temperature for 30 min each. The signals were detected using diaminobenzidine as the chromogen (Liquid DAB-Plus Substrate Kit, Invitrogen), and the sections were counterstained with hematoxylin. Finally, the tissues were dehydrated in ethanol and xylene, and mounted for evaluation.

The metastatic tumor nodules in mice lungs were verified using HE stain. Before HE stain being conducted, the tissues were deparaffinized and rehydrated. The sections were washed in 1x phosphate-buffered saline (PBS), rinsed in ddH<sub>2</sub>O, and stained with hematoxylin solution. After washing in tap water, the sections were rinsed in 1x PBS and 95% ethanol, and stained with eosin solution. Finally, the sections were immersed in 95%, 100% ethanol and xylene, and mounted for evaluation.

Before performing ICC/IF, coverslips were acid cleaned by incubating them in 1M HCl for 24 h to remove any dust that can cause artifacts. After rinsing them three times in ddH<sub>2</sub>O and 95% ethanol, coverslips were submerged in the 0.1 mg/ml solution of gelatin or poly-L-lysine for 5 min, air-dried and sterilized in a culture hood under UV light for a minimum of 2 h. Coating coverslips will improve the cell's adhesion to the glass. After seeding adherent cells on coverslips and incubating them at 37°C overnight, cells were fixed with 4% formaldehyde (10% formalin) for 10 min at room temperature, and washed three times with 1x PBS. If probing for a target whose epitope is expressed intracellularly, cellular permeabilization is necessary. Permeabilization was performed by treating cells with 0.5% Triton X-100 in 1x PBS for 10 min at room temperature. Following washing cells, blocking unspecific binding sites was conducted with 2% bovine serum albumin (BSA) in 1x PBS for 2 h at room temperature. The primary antibodies diluted in the blocking buffer were added, and cells were incubated at 4°C overnight. After washing cells four times (15 min per time) with 1x PBS and shaking, the fluorescent secondary antibodies were added, and cells were incubated at room temperature for 2 h. Cells were washed four times, and then nuclear labeling was stained with 4',6-diamidino-2-phenylindole (DAPI, SIGMA). After rinsing cells with 1x PBS, coverslips were mounted onto slides with Fluoromount-G (SouthernBiotech, Birmingham, AL) and examined under a

fluorescent microscope (BX51, Olympus, Tokyo, Japan).

### **MTT assay and luciferase-reporter assay**

In 24-well plates,  $5 \times 10^3$  cells were seeded in 500  $\mu$ l of medium per well, and cell growth was evaluated for 1-5 days using the MTT assay. At the time point each day, the culture medium was removed and the cells were washed using 1x PBS. Subsequently, 500  $\mu$ l of MTT solution (0.5 mg/ml, MDBio, New Taipei, Taiwan) was added to each well, and the plate was incubated at 37°C for 3 h. After washing the cells, 400  $\mu$ l of DMSO (J.T. Baker, Austin, TX) was added, and the plate was placed on a table shaking at 150 rpm for 5 min to thoroughly dissolve the formazan (MTT metabolic product) in the solvent. Finally, the optical density of 100  $\mu$ l solution at 570 nm was recorded in triplicate, which should be directly correlated with the number of cells.

The luciferase assay was conducted using a Dual-Luciferase<sup>®</sup> Reporter Assay System (Promega, Madison, WI). For the luciferase assay, cells were seeded into 6-well plates. TOPflash and FOPflash constructs (Upstate, Charlottesville, VA) were respectively co-transfected with a Renilla luciferase plasmid (Promega) as the internal control to normalize for transfection efficiency. At 48 h post-transfection, the cells were lysed in 500  $\mu$ l 1x PLB, and the dual-luciferase assay was performed according

to the manufacturer's protocol.

### **Wound-healing, migration and invasion assays**

For the wound-healing assay,  $1 \times 10^4$ - $4 \times 10^4$  cells in 100  $\mu$ l of culture medium were seeded into each well of Culture-Insert (Ibidi, GmbH, München, Germany) and cultured overnight to form a confluent monolayer. After removing the insert, a cell-free gap of 500  $\mu$ m in width was created. To evaluate the migratory abilities of cells, the area containing the gap was photographed using a light microscope at different time points during culture.

The migration assay was performed using a 24-well transwell system with 8- $\mu$ m pores in the PET membranes (BD Biosciences). For the migration assay, the cells were trypsinized and suspended in serum-free medium. Each transwell-cup was filled with 300  $\mu$ l cell suspensions ( $1 \times 10^6$  cells/ml), and each well of the 24-well plates was filled with 800  $\mu$ l of culture medium containing 10% FBS. After placing cups in wells, cells were cultured at 37°C for 7-18 h. The non-migrating cells were removed from the upper surface of the membrane, and the lower side of the filter membrane was fixed using 10% formalin and stained using 10% Giemsa reagent (MERCK, Darmstadt, Germany) for 5 min. Finally, the cells that had migrated were washed using 1xPBS and counted using bright-field microscopy.

For the invasion assay, the filter membranes of the transwell-cups were first coated with Matrigel (BD Biosciences). The cells were then manipulated in the same way as in the migration assay and cultured for 24 h.

## Primers

List of the gene-specific primer sequences used in the RT-PCR and qPCR assays:

Assay	Gene	Primer sequences
RT-PCR	HIP1	F 5'-GTTGTGGCCTCAACCATT-3'
		R 5'-ACCACTTCTTGCAGTGTAG-3'
	GAPDH	F 5'-CCACCCATGGCAAATTCCATGGCA-3'
		R 5'-TCTAGACGGCAGGTCAGGTCCACC-3'
qPCR	E-cadherin	F 5'-CAAGCTCATGGATAACCAGAATA-3'
		R 5'-CAAGAATTCCTCCAAGAATCCC-3'
	MITF	F 5'-GTGTCCCCACAAAATGGGA-3'
		R 5'-GGCTGCTTGTTTTGGAAGCT-3'
	Snail	F 5'-ACCACTATGCCGCGCTCTT-3'
		R 5'-GGTCGTAGGGCTGCTGGAA-3'
	Slug	F 5'-TTCGGACCCACACATTACCT-3'
		R 5'-GCAGTGAGGGCAAGAAAAG-3'

	Vimentin	F	5'-CTCTTCCAAACTTTTCCTCCC-3'
		R	5'-AGTTTCGTTGATAACCTGTCC-3'
	FAK	F	5'-TCCCTATGGTGAAGGAAGT-3'
		R	5'-TTCTGTGCCATCTCAATCT-3'
	PAI1	F	5'-CTTCACGAGTCTTTCAGACC-3'
		R	5'-GCTGAGACTATGACAGCTGT-3'
	TNFR1	F	5'-ACTACTACTAAGCCCCTGGC-3'
		R	5'-ATAGGTGGAGCTGGAGGTGA-3'
	MMP1	F	5'-GGCTGAAAGTGAAGTGGGAAACC-3'
		R	5'-TGCTCTTGGCAAATCTGGCGTG-3'
	GAPDH	F	5'-TGAAGGTCGGAGTCAACGGATT-3'
		R	5'-CCTGGAAGATGGTGATGGGATT-3'

### Antibodies

List of the specific primary antibodies used in the Western blot (WB), coimmunoprecipitation (co-IP), immunohistochemistry (IHC) and immunocytochemistry (ICC)/immunofluorescence (IF) assays:

Assay	Antibody	Catalog # and Manufacturer
WB	HIP1 (4B10)	#sc-47754, Santa Cruz, Santa Cruz, CA

	$\alpha$ -tubulin	#T5168, SIGMA, St Louis, MO
	Snail	#H00006615-M10, Novus, Littleton, CO
	Slug	#H00006591-M04, Novus
	Vimentin	#550513, BD Biosciences, San Jose, CA
	E-cadherin	#610182, BD Biosciences
	$\beta$ -catenin	#sc-7963, Santa Cruz
	Lamin A/C	#sc-7292, Santa Cruz
	GSK3 $\beta$	#610202, BD Biosciences
	pGSK3 $\beta$ -Ser9	#9336, Cell Signaling, Danvers, MA
	Akt	#9272, Cell Signaling
	pAkt-Thr308	#4056, Cell Signaling
	pAkt-Ser473	#9271, Cell Signaling
	PDK1	#3062, Cell Signaling
	pPDK1-Ser241	#3061, Cell Signaling
	PI3K p85	#4257, Cell Signaling
	pPI3K p85-Tyr458/p55-Tyr199	#4228, Cell Signaling
co-IP	HIP1 (4B10)	#sc-47754, Santa Cruz
	Akt	#9272, Cell Signaling
IHC	HIP1 (1F12)	#H00003092-M01, Novus

	human mitochondria	#ab92824, Abcam, La Jolla, CA
ICC/IF	pAkt-Ser473	#9271, Cell Signaling

### Statistical analysis

All of the statistical analyses were performed using SPSS software. The data are expressed as the mean values  $\pm$  standard deviation (SD). To analyze the results of three independent experiments, a two-tailed, unpaired Student's *t*-test was used. Differences were considered to be statistically significant when the *p* value was  $<0.05$  ( $*p<0.05$ ;  $**p<0.01$ ; and  $***p<0.001$ ). The survival curves were obtained using the Kaplan-Meier method.

### Supplementary figure legends

**Figure E1.** The HIP1 expression levels of clinical specimens in three cohorts were detected using IHC. (A) The standard scale for IHC scoring ranged from 0 to 3. The intensity of the brown color indicated the level of HIP1 expression. (B) HIP1 staining was performed on the lung sections of normal and tumor tissues. (C) The percentage of low and high HIP1 expressing tissues was detected in the normal alveolar epithelium/AdCA and the normal bronchial epithelium/SCC. (D-G) Low-level HIP1 expressions significantly correlated with poor survival of AdCA and SCC patients in the first cohort. (H) In the NSCLC patients receiving chemotherapy from the first cohort, low HIP1 expression levels significantly correlated with poor overall survival. (I-N) In the second cohort, the NSCLC and AdCA patients showed correlation between low HIP1 expression levels and poor survival, but SCC patients did not. (O-Q) In the third cohort, the low HIP1 expression levels significantly correlated with poor overall survival in AdCA patients, but not in SCC.

**Figure E2.** The low-level HIP1 mRNA expression significantly correlated with poor overall and disease-free survival of NSCLC patients. (A-G) Survival curves based on HIP1 data were collected from the Prognoscan database.

**Figure E3.** HIP1 expression reversely correlated with AdCA cellular mobility. (A)

The endogenous HIP1 expression levels of various AdCA cell lines were detected using WB, and xenografts were evaluated using IHC. (B) Transiently decreasing HIP1 expression increased the migratory and invasive abilities of CL1-0 cells, as assessed in WB, migration and invasion assays. (C) Transiently increasing HIP1 expression decreased the migratory and invasive abilities of CL1-5 cells, as assessed in WB, migration and invasion assays.  $\alpha$ -tubulin was used as the internal control of WB. The intensity of the brown color reflected the level of HIP1 expression in xenografts.

**Figure E4.** Stable HIP1 knockdown in A549 cells significantly repressed cell growth and promoted cellular mobility. (A) HIP1 expression levels were evaluated using WB. Cell growth was evaluated using MTT. (B) The mRNA expressions of EMT markers were evaluated using qPCR. (C) The protein expression levels of EMT markers were evaluated using WB. (D) The migratory ability was evaluated using the wound-healing assay. (E) The migratory ability was evaluated using the migration assay. (F) The invasive ability was evaluated using the invasion assay. GAPDH was used as the internal control for qPCR.  $\alpha$ -tubulin was used as the internal control for WB.

**Figure E5.** Stable HIP1 knockdown in H441 cells significantly promoted cellular

mobility. (A) HIP1 expression levels were evaluated using WB. Cell growth was evaluated using MTT. (B) The mRNA expressions of EMT markers were evaluated using qPCR. (C) The protein expressions of EMT markers were evaluated using WB. (D) The migratory ability was evaluated using the wound-healing assay. (E) The migratory ability was evaluated using the migration assay. (F) The invasive ability was evaluated using the invasion assay. (G) HIP1 expressions were evaluated in the transiently HIP1-overexpressing H441 cells using WB. (H) The cellular mobility of the transiently HIP1-overexpressing H441 cells was evaluated using the migration and invasion assays. GAPDH was used as the internal control for qPCR.  $\alpha$ -tubulin was used as the internal control for WB.

**Figure E6.** Stable HIP1 overexpression in H928 cells significantly repressed cellular mobility. (A) HIP1 expressions were detected using WB. Cell growth was detected using MTT. (B) The mRNA expression levels of EMT markers were detected using qPCR. (C) The protein expression levels of EMT markers were detected using WB. (D) The migratory ability was detected using the wound-healing assay. (E) The migratory ability was detected using the migration assay. (F) The invasive ability was detected using the invasion assay. GAPDH was used as the internal control for qPCR.  $\alpha$ -tubulin was used as the internal control for WB.

**Figure E7.** Stable HIP1 overexpression in H1299 cells significantly promoted cell growth and repressed cellular mobility. (A) HIP1 expression levels were detected using WB. Cell growth was detected using MTT. (B) The mRNA expression levels of EMT markers were detected using qPCR. (C) The protein expression levels of EMT markers were detected using WB. (D) The migratory ability was detected using the wound-healing assay. (E) The migratory ability was detected using the migration assay. (F) The invasive ability was detected using the invasion assay. (G) HIP1 expression levels were detected in the transiently HIP1-knockdown H1299 cells using WB. (H) The cellular mobility of the transiently HIP1-knockdown H1299 cells was detected using the migration and invasion assays. GAPDH was used as the internal control for qPCR.  $\alpha$ -tubulin was used as the internal control for WB.

**Figure E8.** Decreased HIP1 expression in CL1 cells promoted distant metastasis to livers and kidneys *in vivo*. (A) Mice receiving orthotopic lung injection of the CL1-0 shHIP1#1 and CL1-5 Vec cells with low HIP1 expression levels exhibited distant metastasis to liver. (B) Mice receiving orthotopic lung injection of the CL1-0 shHIP1#1 and CL1-5 Vec cells with low HIP1 expression levels exhibited distant metastasis to kidney. (C) No significant differences in lung weight were detected

between the HIP1-manipulated CL1-0 and CL1-5 groups.

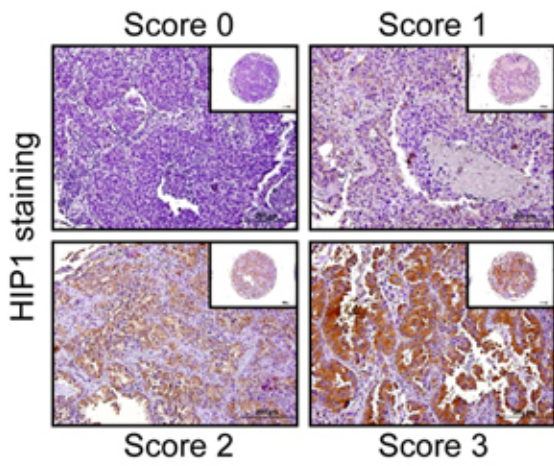
**Figure E9.** HIP1 downregulation in H157 cells promoted cellular mobility. (A) HIP1 expression levels were evaluated using WB. (B-D) The migratory and invasion abilities of H157-Vec, H157-HIP1, H157-scramble, H157-shHIP1#1, and H157-shHIP1#2 cells were evaluated using migration and invasion assays.  $\beta$ -actin was used as the internal control for WB.

**Figure E10.** HIP1 downregulation in SK-EMS-1 cells promoted cellular mobility. (A) HIP1 expression levels were evaluated using WB. (B-D) The migratory and invasion abilities of SK-EMS-1-Vec, SK-EMS-1-HIP1, SK-EMS-1-scramble, SK-EMS-1-shHIP1#1, and SK-EMS-1-shHIP1#2 cells were evaluated using migration and invasion assays.  $\beta$ -actin was used as the internal control for WB.

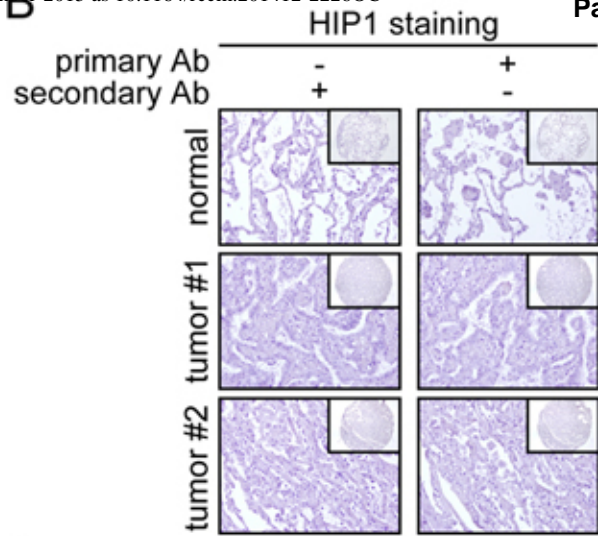
Table E1. The Association of HIP1 expressions with NSCLC prognosis of patients in four cohorts from Prognoscan database

Dataset	Cohort	Cancer type	End point	N	Array type	Probe ID	HR [95% CI <sup>low</sup> - CI <sup>upp</sup> ]	Cox <i>p</i> -value
GSE31210	NCCRI	Lung cancer Adenocarcinoma	Overall Survival	204	HG-U133_Plus_2	226364_at	0.35 [0.17 - 0.70]	0.0030
GSE31210	NCCRI	Lung cancer Adenocarcinoma	Disease-Free Survival	204	HG-U133_Plus_2	226364_at	0.40 [0.24 - 0.68]	0.0006
GSE31210	NCCRI	Lung cancer Adenocarcinoma	Overall Survival	204	HG-U133_Plus_2	205425_at	0.44 [0.22 - 0.92]	0.0282
GSE13213	Nagoya (1995-1999, 2002-2004)	Lung cancer Adenocarcinoma	Overall Survival	117	G4112F	A_23_P71033	0.68 [0.47 - 0.97]	0.0323
jacob-00182- CANDF	CAN/DF	Lung cancer Adenocarcinoma	Overall Survival	82	HG-U133A	205425_at	0.38 [0.16 - 0.93]	0.0341
jacob-00182- CANDF	CAN/DF	Lung cancer Adenocarcinoma	Overall Survival	82	HG-U133A	205426_s_at	0.31 [0.10 - 0.97]	0.0439
GSE8894	Seoul (1995-2005)	Lung cancer NSCLC	Disease-Free Survival	138	HG-U133_Plus_2	1560317_s_at	0.00 [0.00 - 0.50]	0.0304

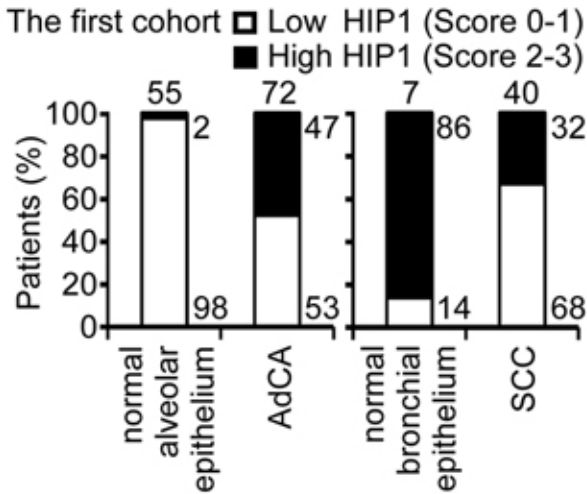
**A**



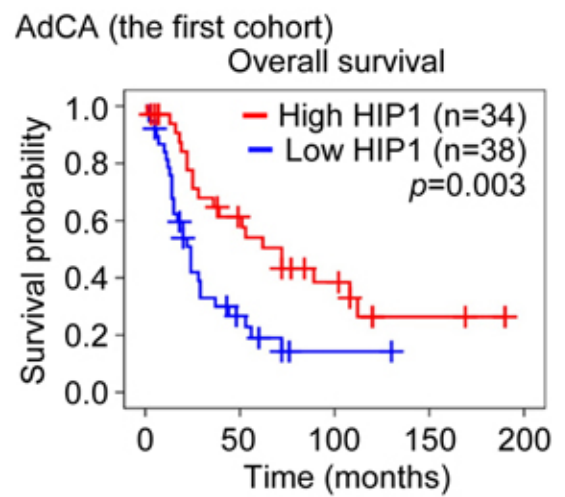
**B**



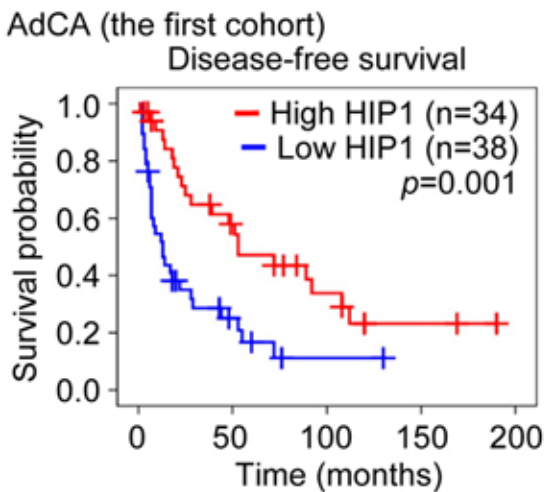
**C**



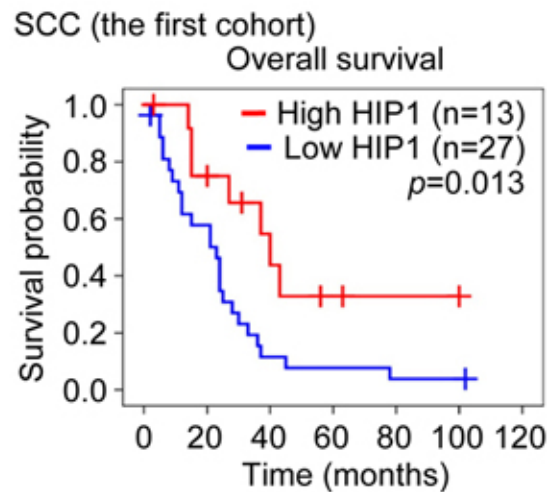
**D**



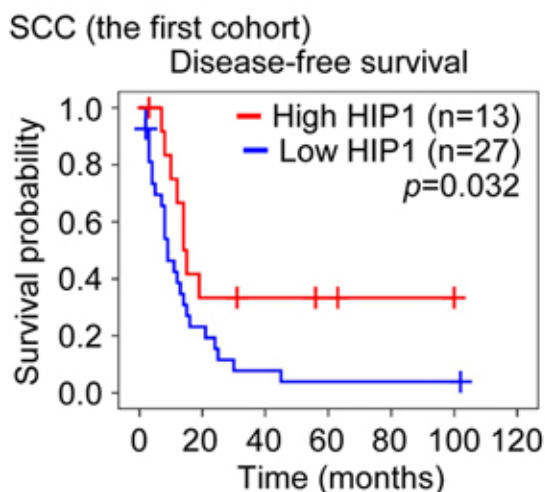
**E**



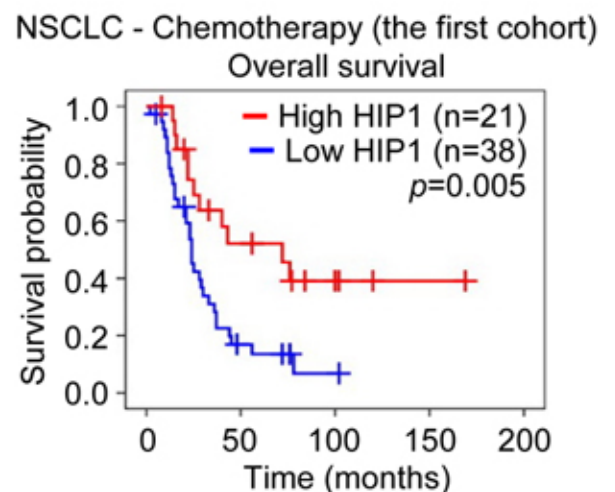
**F**



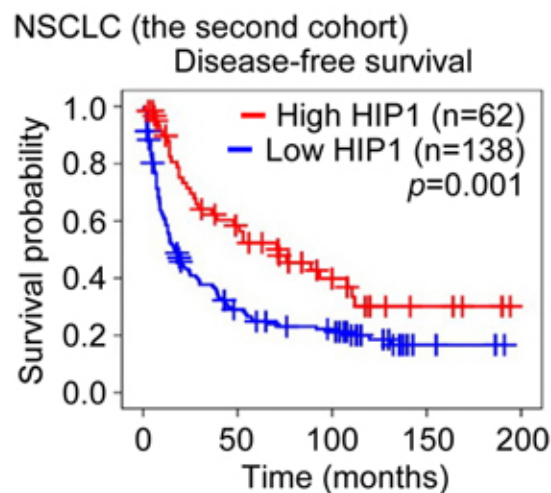
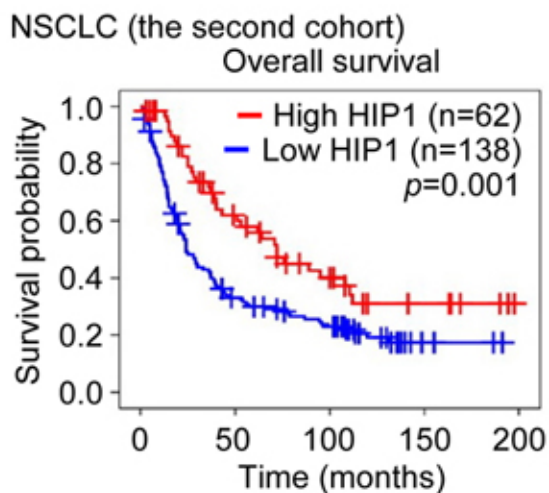
**G**



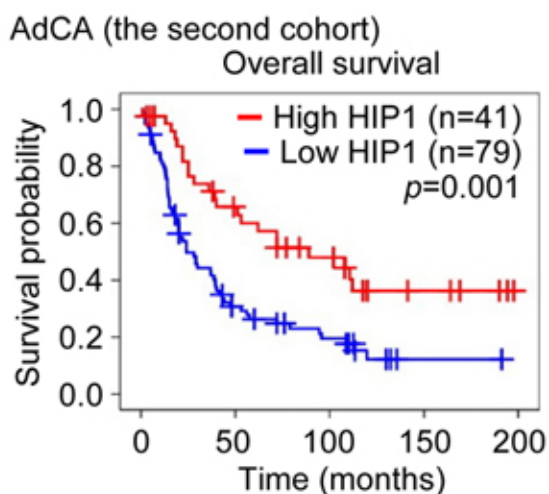
**H**



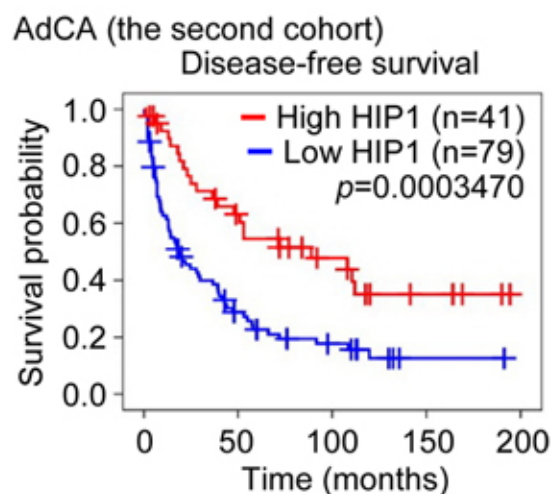
J



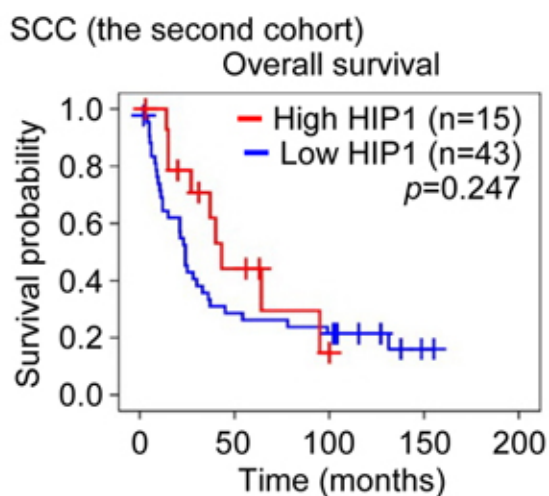
K



L



M



N

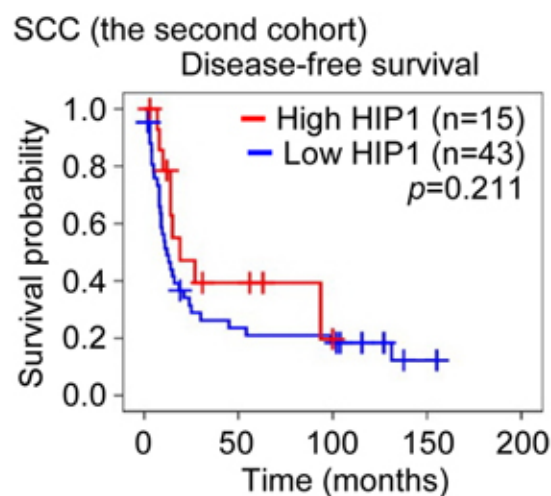
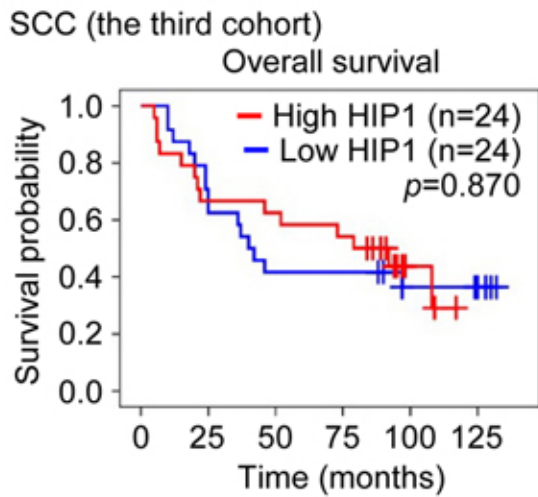
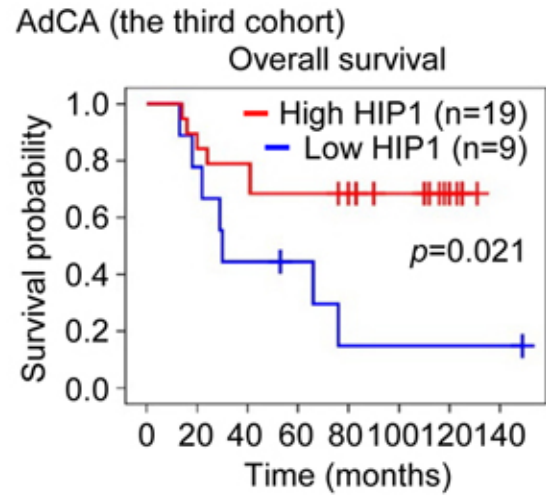
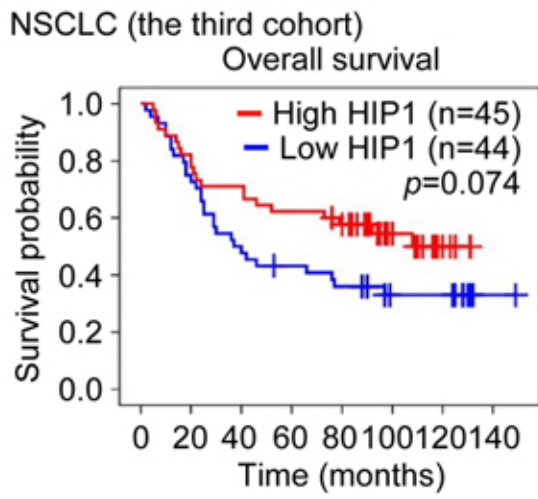


Figure E1 (Hsu et al)



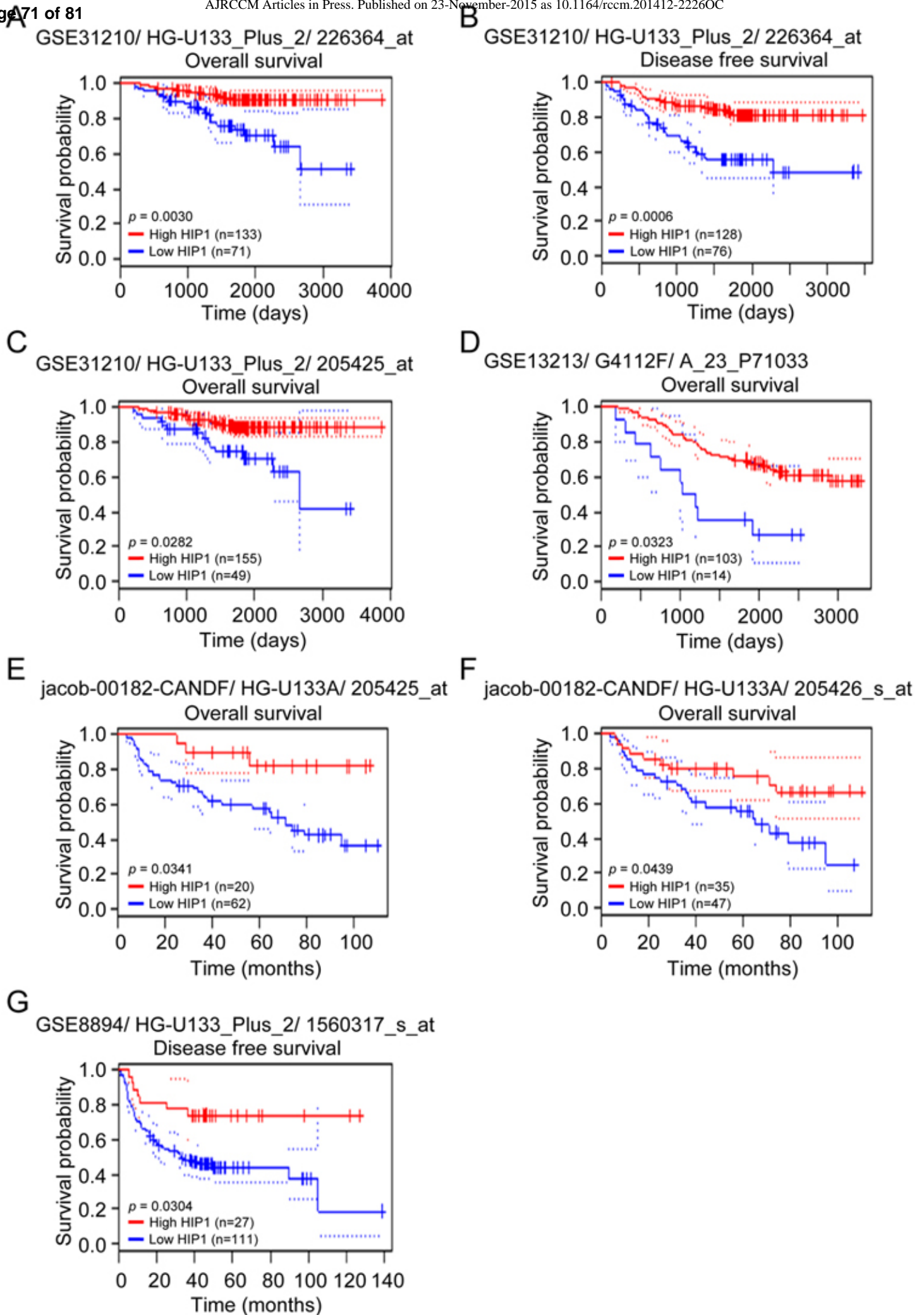
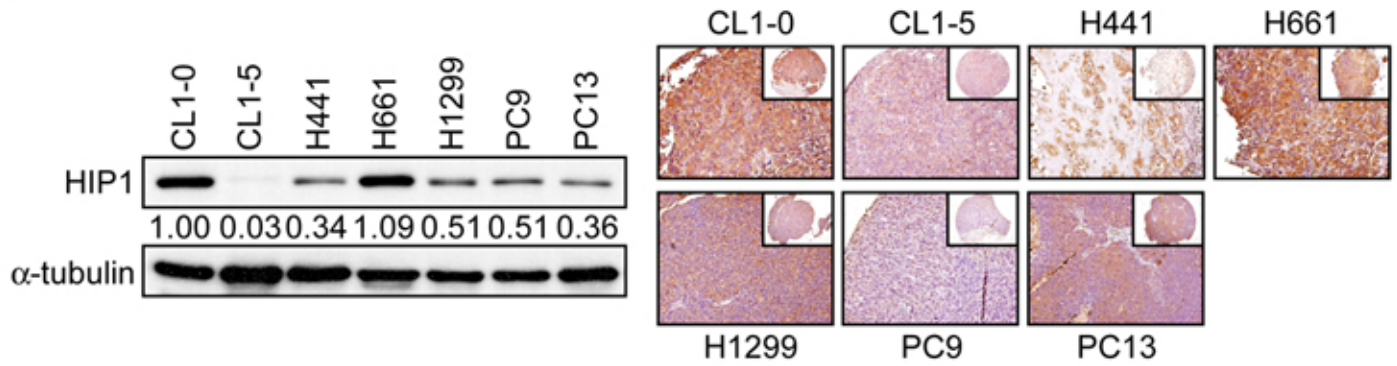
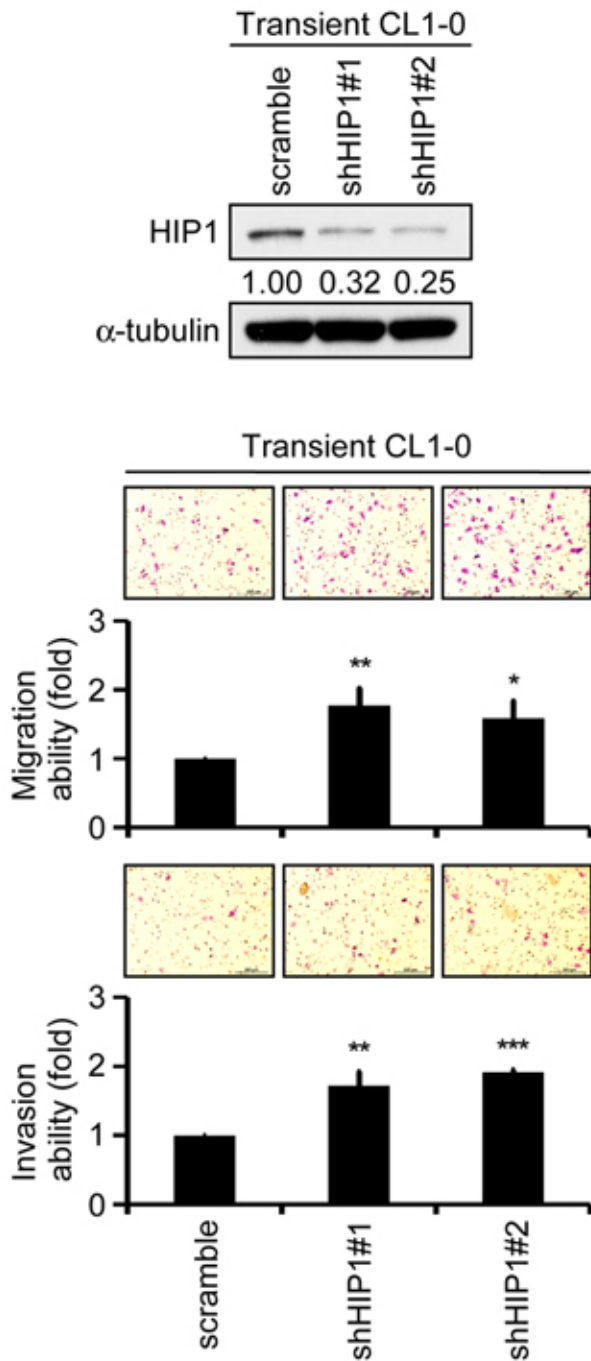


Figure E2 (Hsu et al.)

A



B



C

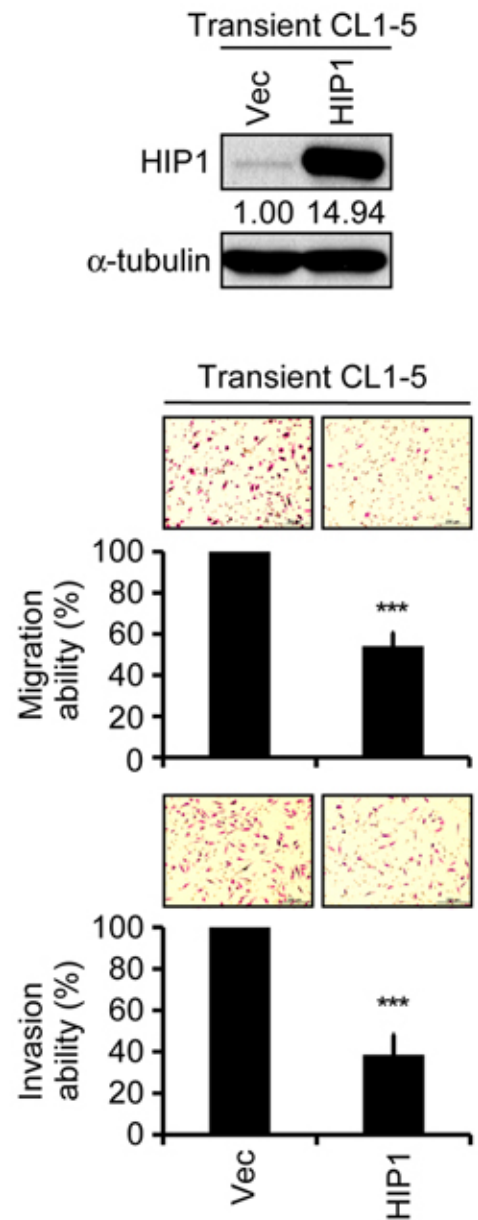


Figure E3 (Hsu et al.)

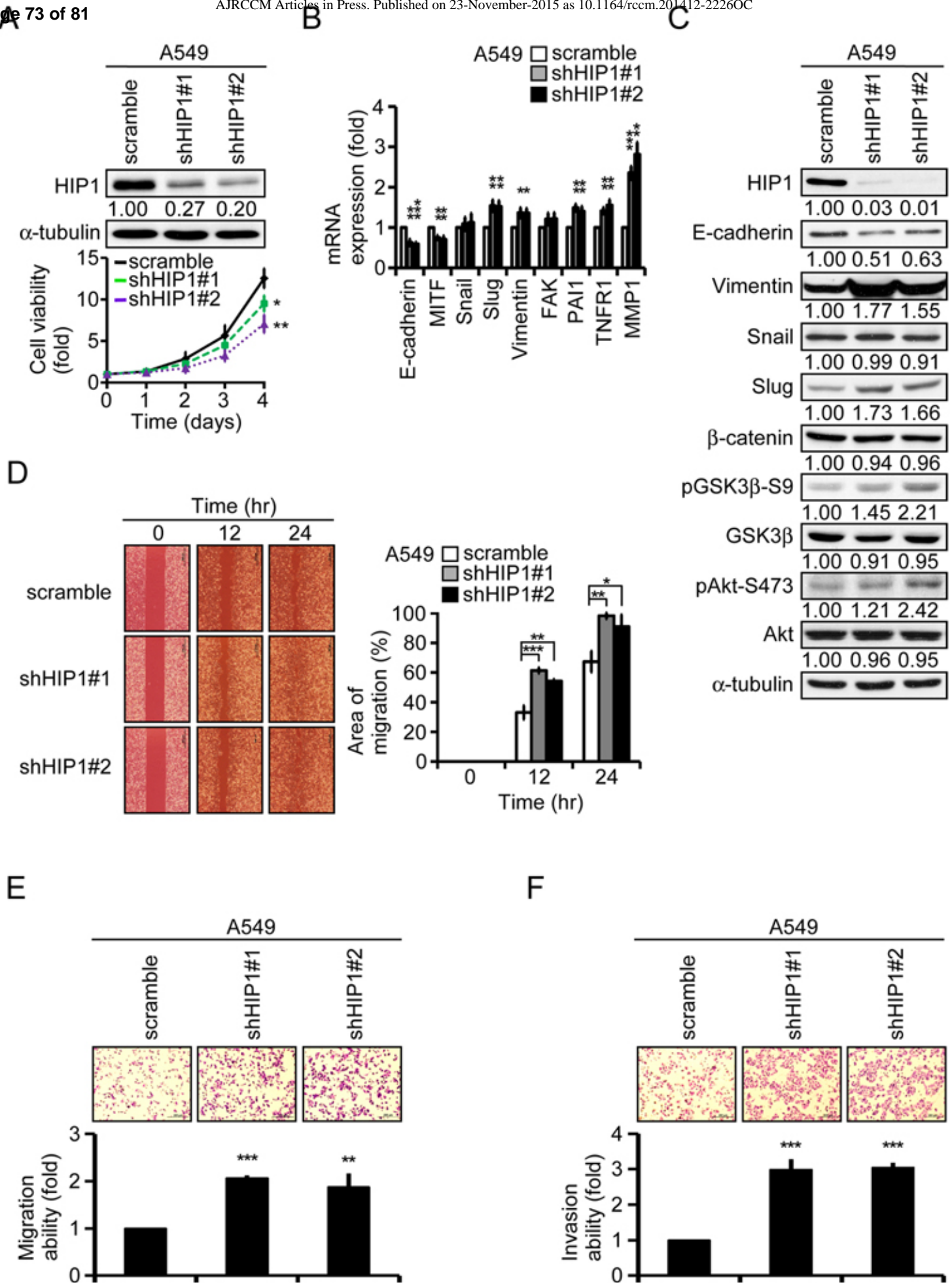


Figure E4 (Hsu et al.)

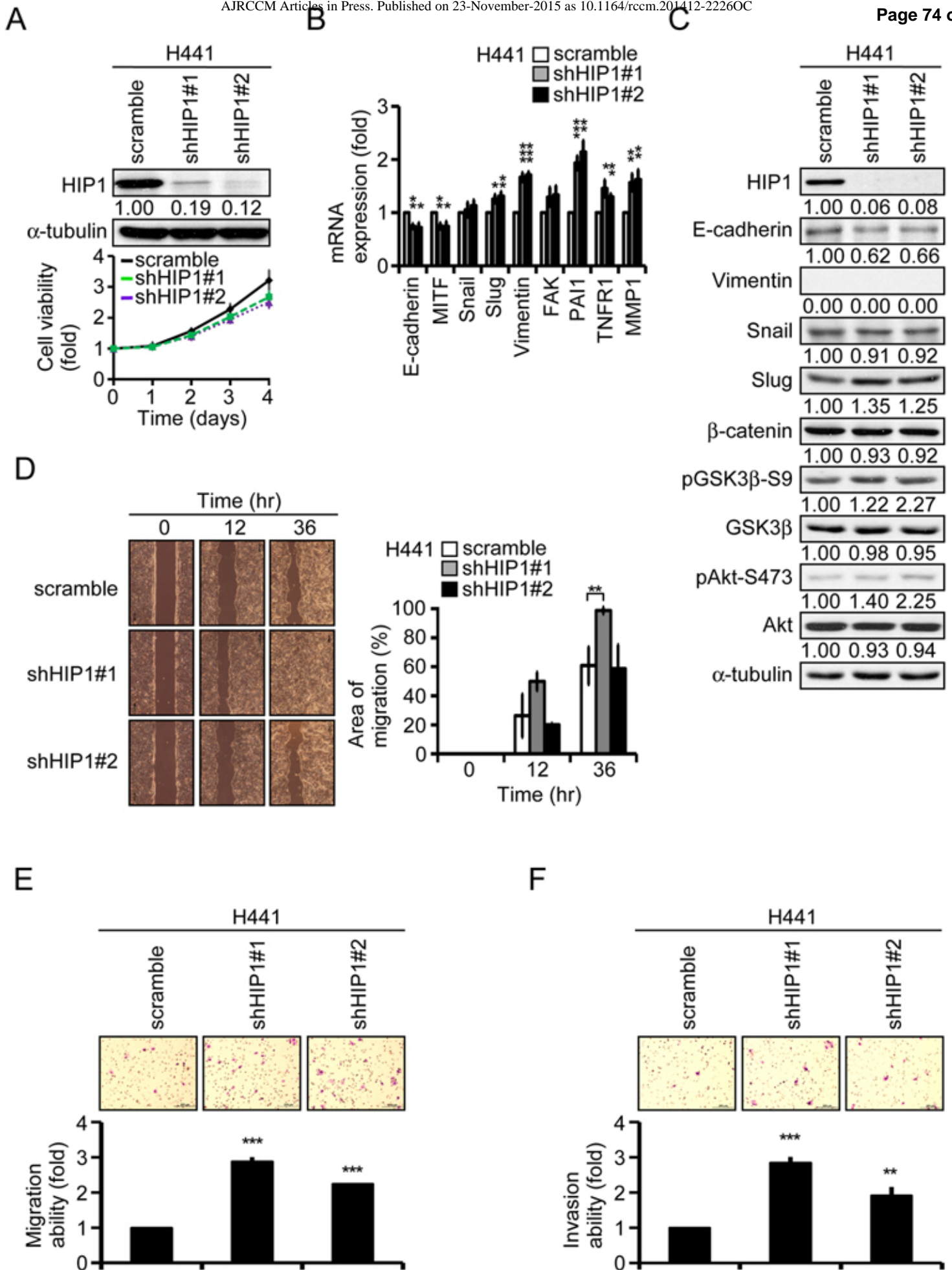


Figure E5 (Hsu et al.)

H

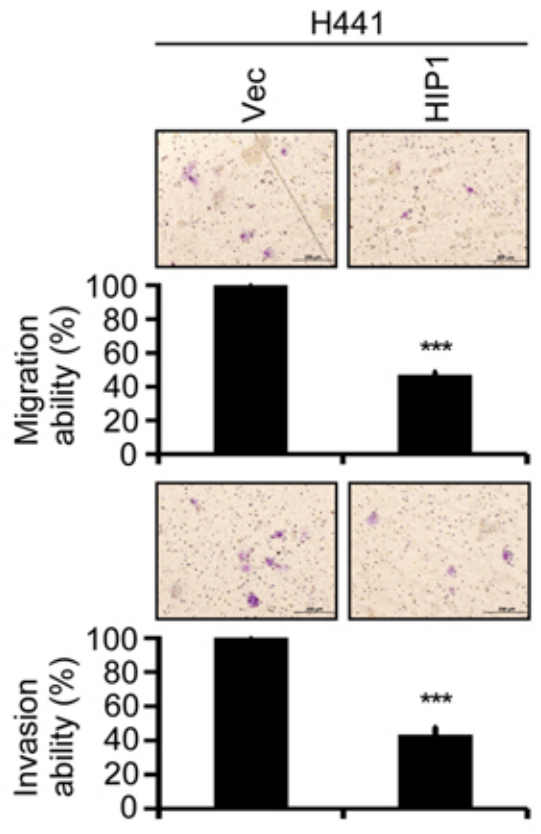
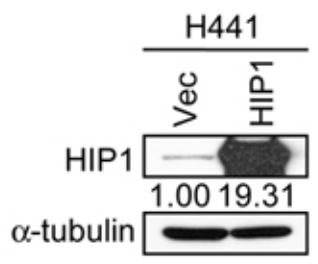


Figure E5 (Hsu et al.)

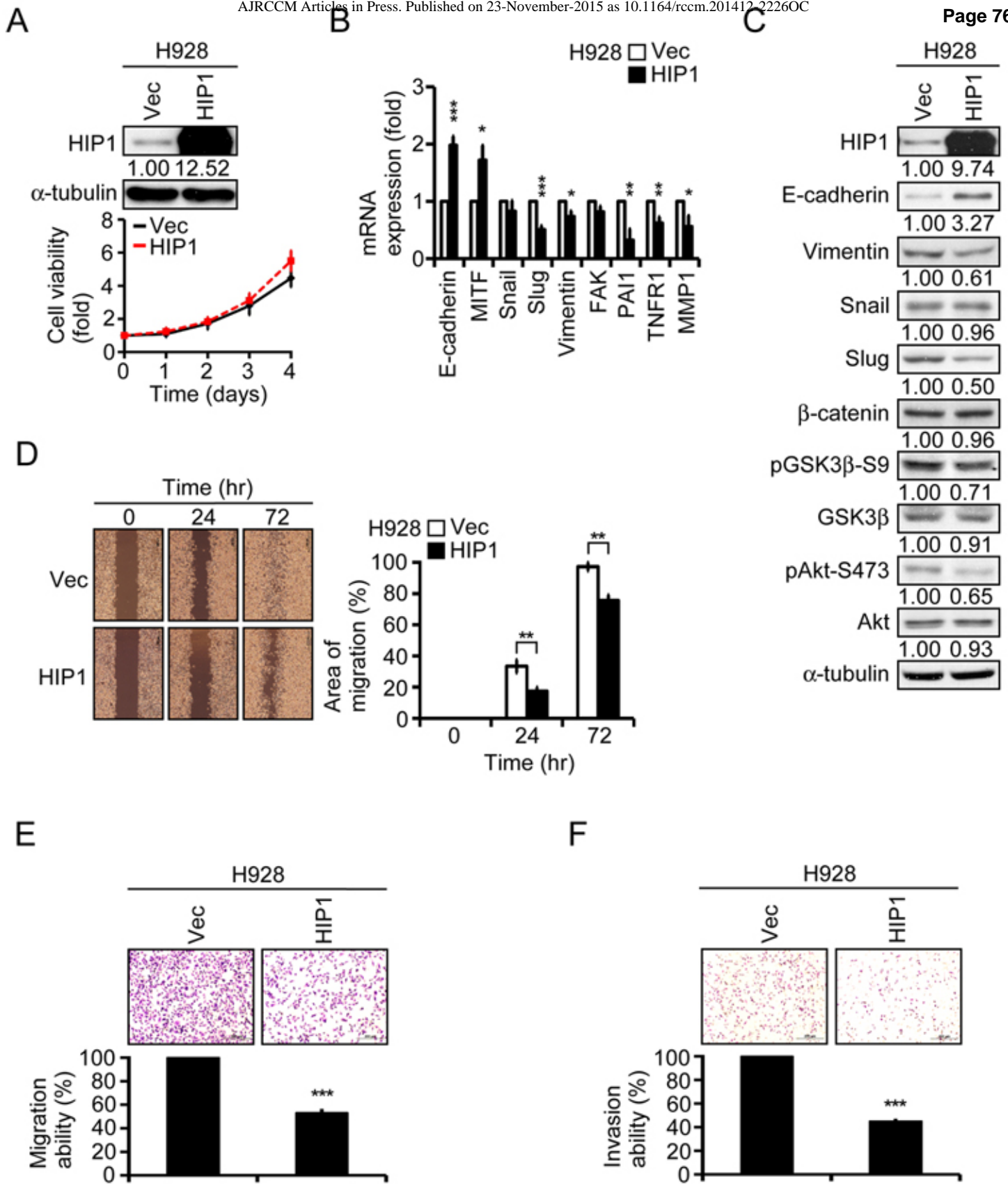


Figure E6 (Hsu et al)

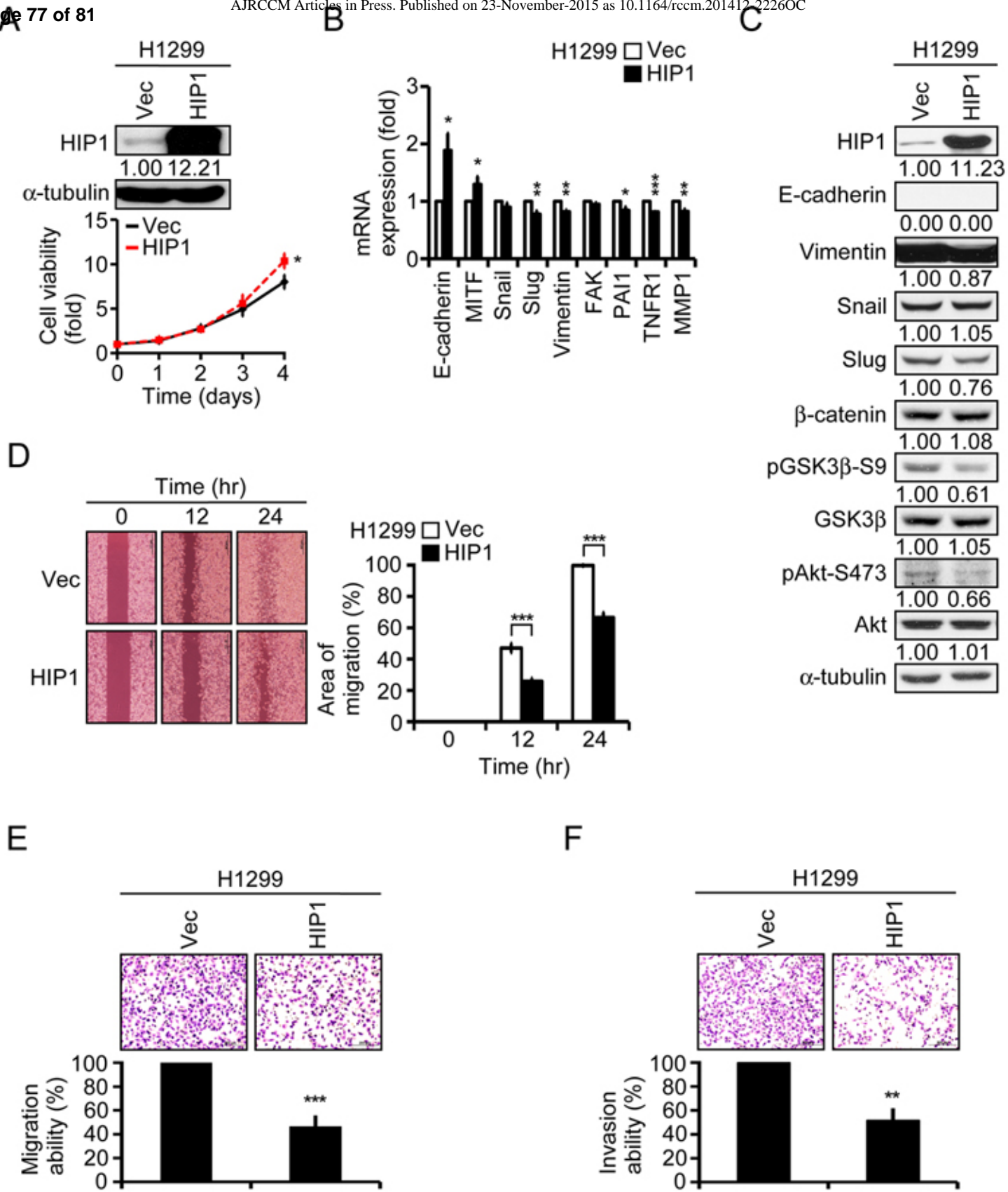
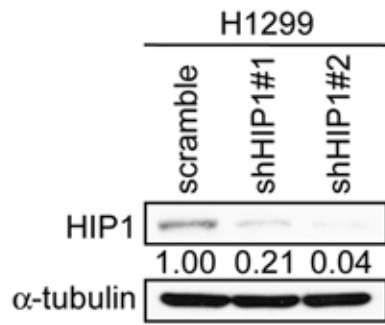


Figure E7 (Hsu et al.)

G



H

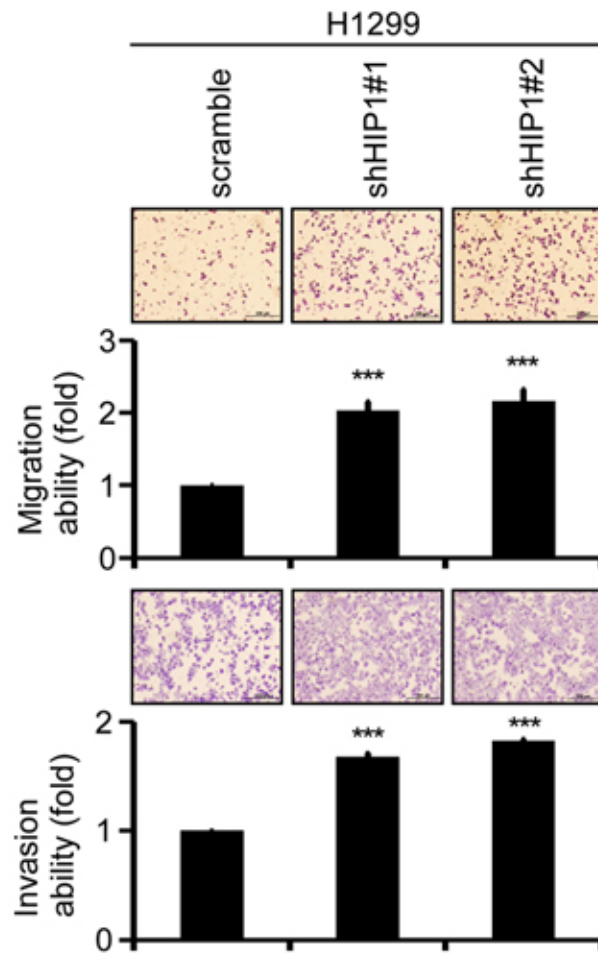


Figure E7 (Hsu et al.)

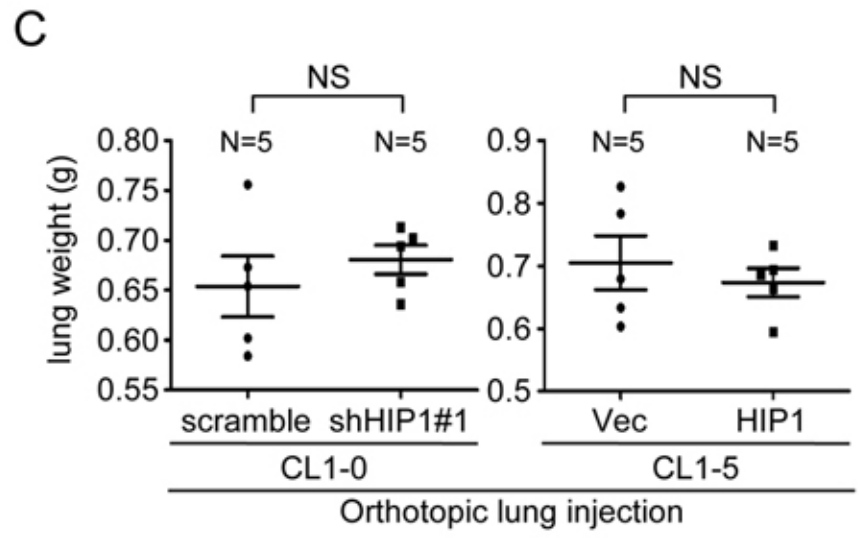
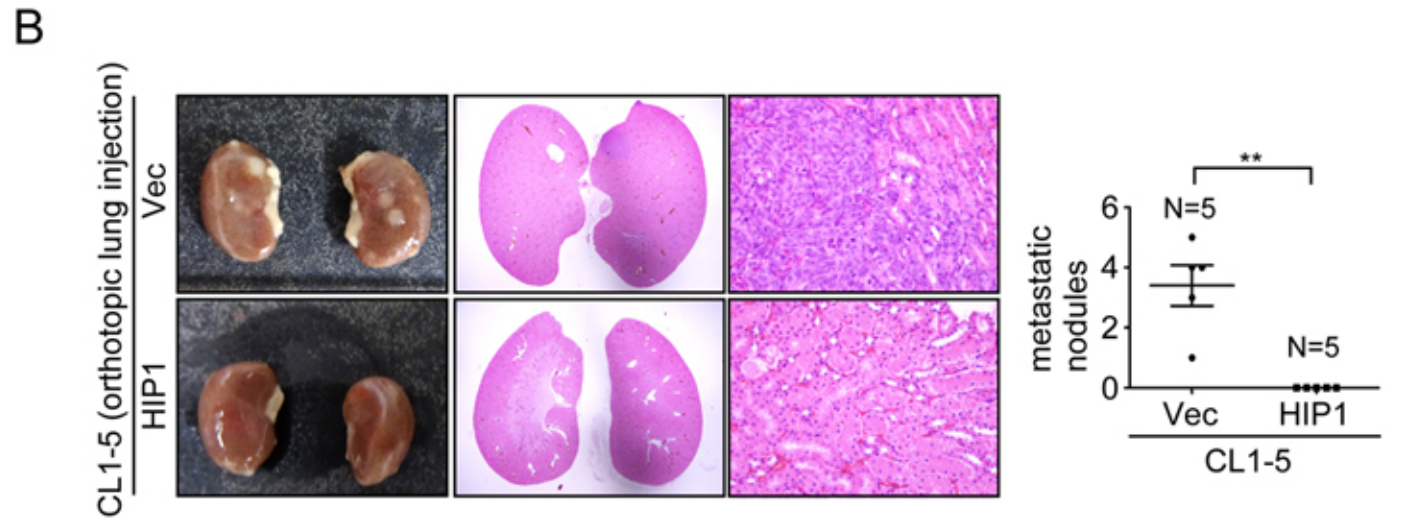
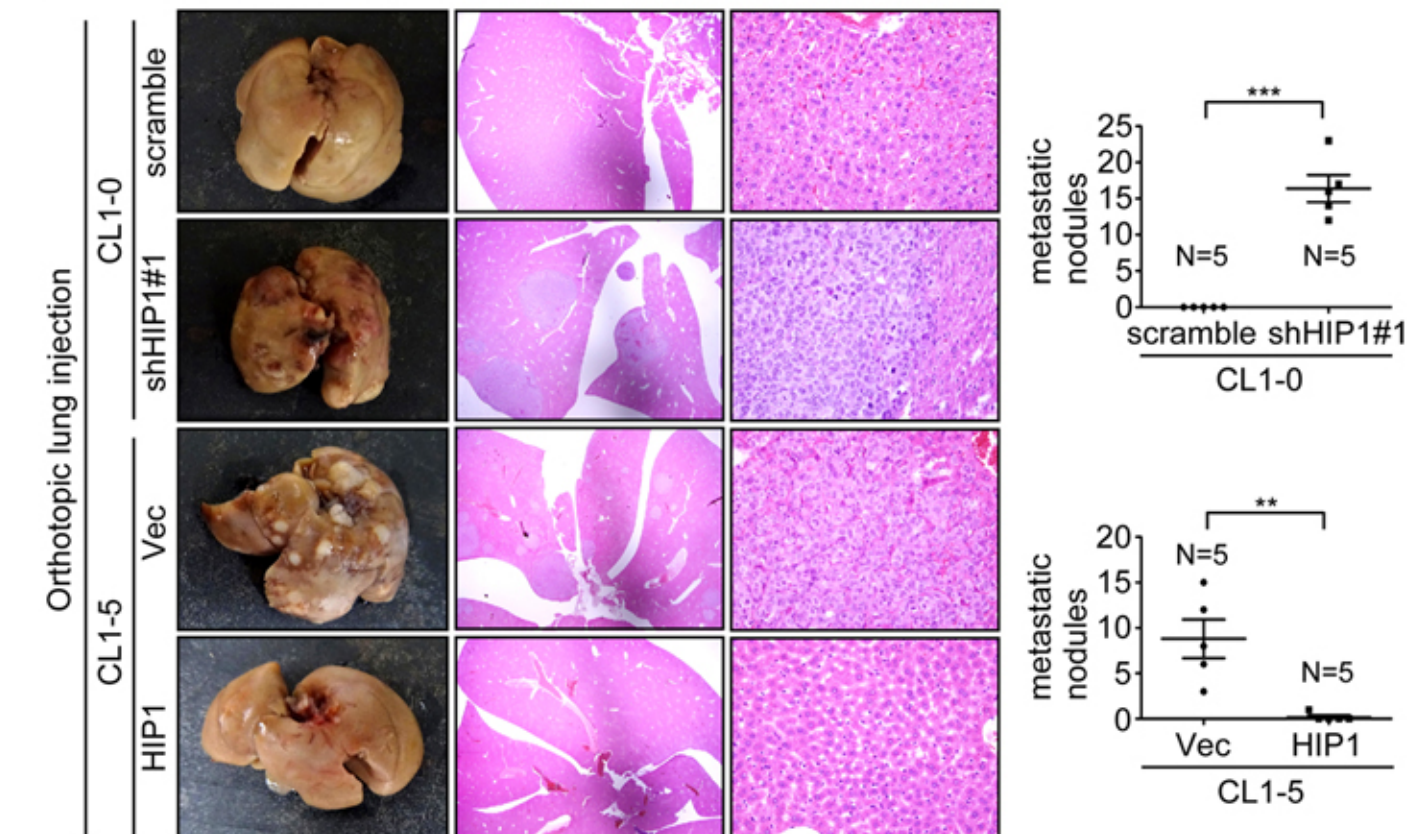


Figure E8 (Hsu et al.)

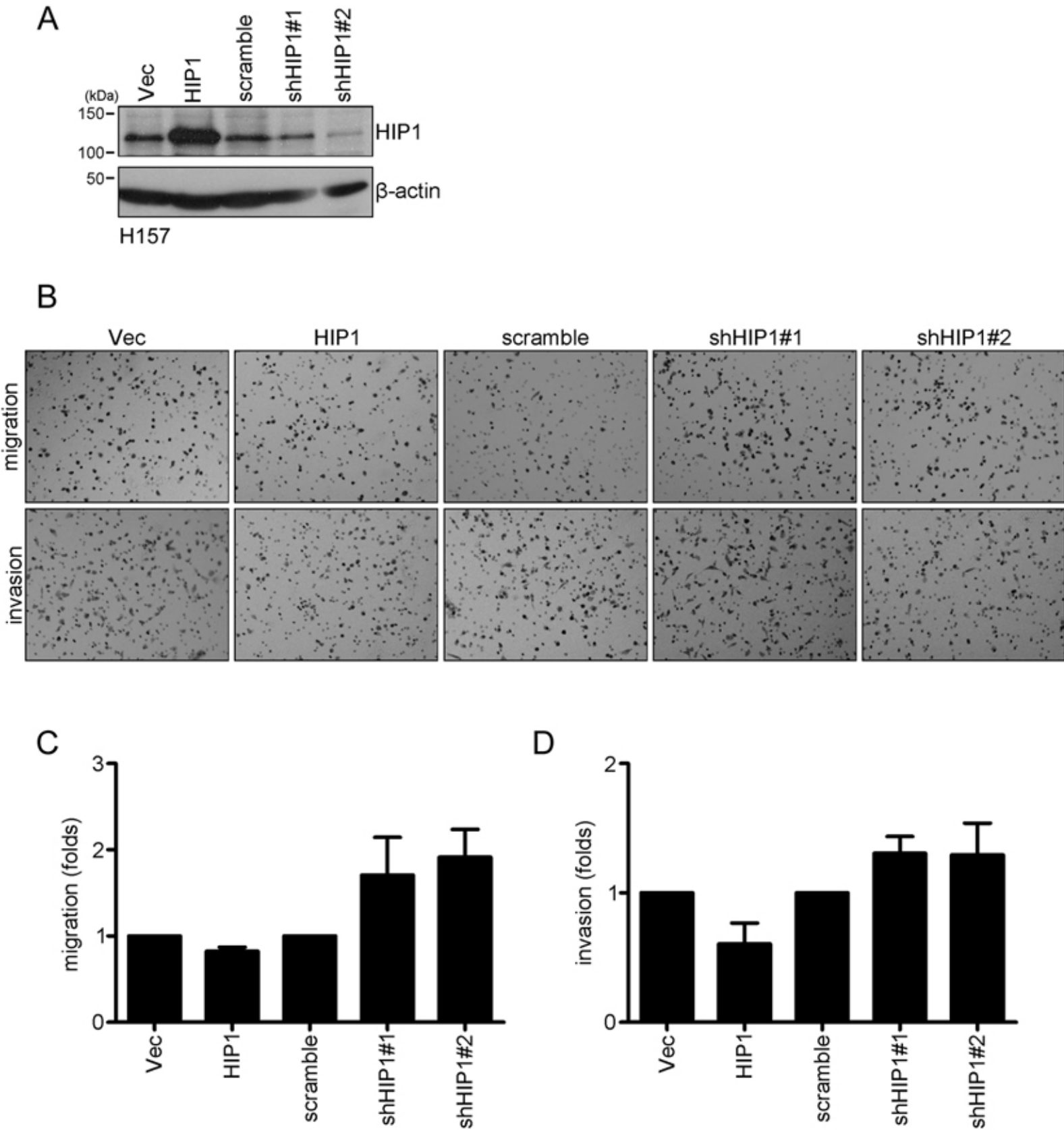
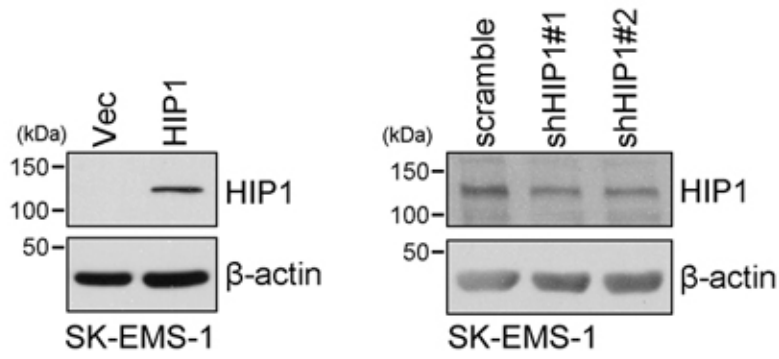
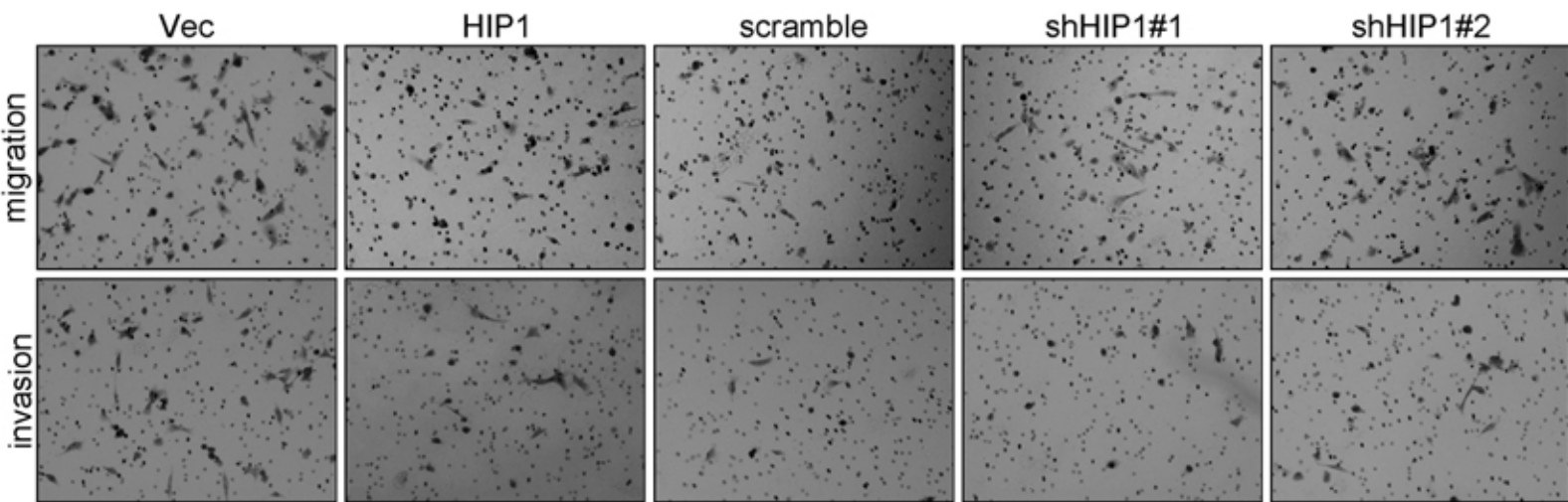


Figure E9 (Hsu et al.)

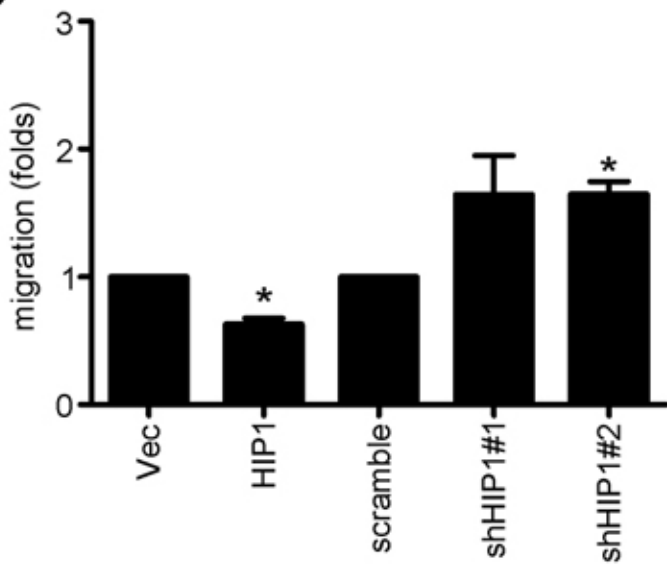
A



B



C



D

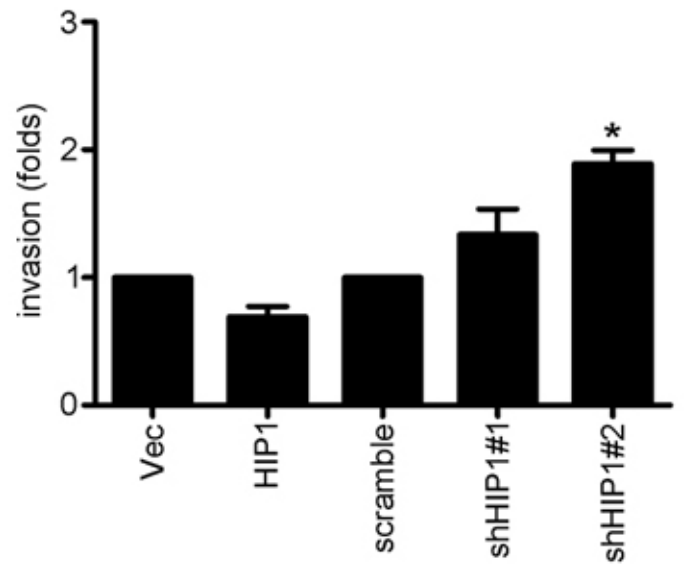


Figure E10 (Hsu et al.)